Pion-nucleus inelastic scattering: Reaction contributions and nuclear spin determinations

E. R. Siciliano*

Meson Physics Division, Los Alamos National Laboratory, Los Alamos, New Mexico 87545

G. E. Walker

Physics Department, Indiana University, Bloomington, Indiana 47405
(Received 29 January 1981)

Formulas for pion-nucleus inelastic scattering are presented in a form that may suggest experiments to isolate various contributions to the reaction, including S-wave, P-wave spin and nonspin flip, and effects of nucleon Fermi motion. Adopting a form of the distorted wave impulse appoximation, we obtain an expression for inelastic cross sections that clearly separate the pion laboratory energy (E), three-momentum transfer (q), and scattering angle (θ) dependences. The result is similar to the separation of longitudinal and transverse form factors in inelastic electron scattering. By varying the energy of the incident pion, but working at fixed q, one can determine whether a given nuclear excitation has natural or unnatural parity. By working at fixed θ, and varying E and thus q, one can isolate different reaction contributions—spin, scalar, and "convection current." We also discuss the potential usefulness of studying the energy dependence of angle-integrated differential cross sections at fixed energy loss. The predictions of our formulas are in good agreement with recent data on natural and unnatural parity excitations in $^{12}C(\pi,\pi')^{12}C^*$. Thus, this approach may be useful in analyzing future data in which the final nuclear spin is uncertain. Future experiments with selective q, E, and θ variations to separate nuclear structure from reaction-mechanism uncertainties are suggested.

NUCLEAR REACTIONS, NUCLEAR STRUCTURE Pion inelastic scattering for $T_\pi \simeq 100$ to 300 MeV; simple formulas for calculating $d\sigma/d\Omega(q, E, \theta)$ either at fixed E or fixed q; effects of Fermi motion.

I. INTRODUCTION

Comparison of available pion inelastic scattering data on light nuclei with theoretical predictions[1-6] has shown that present theoretical approaches based on the distorted wave impulse approximation (DWIA) are most often capable of providing satisfactory fits to the data. Shapes of angular distributions are well predicted and overall renormalization factors, presumably resulting from inadequate nuclear wave functions, appear consistent with those required in electron or proton-nucleus inelastic scattering. The semiquantitative agreement between theory and experiment may, however, seem fortuitous because higher order corrections and special effects, such as crossing associated with pion absorption and reemission, are obviously not small nor are they explicitly contained in the DWIA.

The pion-induced nuclear excitations studied to date have been associated with collective states or final states whose quantum numbers are such that, in a particular region of momentum transfer, they are predicted to be relatively strongly excited because of the particular spin and isospin properties of the pion-nucleon interaction. However, for those states where a one-step DWIA mechanism does not predict strong excitation, multistep processes may well be important. For

such states, comparison of results with data obtained from other projectiles, particularly protons and electrons, is necessary before conclusions regarding nuclear structure can be reached. Of course, it may turn out that some states seen in inelastic pion scattering cannot be easily seen using other projectiles.

Features that would be useful in future (π, π') studies could be determined by explicitly separating the pion laboratory energy (E), three-momentum transfer (q), and scattering angle (θ) dependences of some DWIA expression. Such an expression could be used to give one confidence regarding the dominance of selected reaction contributions and also provide information about the spins and parities of the nuclear excitations under investigation. One purpose of this paper is to provide such a test and apply it in a few examples to demonstrate its scope and predictive power.

In obtaining our results, we have been motivated by the analysis of electron-nucleus scattering. To show how some of the basic ideas have already been useful in this case, we briefly discuss the assumptions associated with and utility of the Rosenbluth plot in inelastic electron-nucleus scattering. The differential cross section for inelastic electron scattering, assuming a single virtual photon exchange (one-step process), can

be written in the form[7]

$$\frac{d\sigma}{d\Omega} = \sigma_{\text{Mott}} \left[F_L^2(q^2) + \left(\tfrac{1}{2} + \tan^2 \frac{\theta}{2} \right) F_T^2(q^2) \right] . \quad (1.1)$$

In obtaining this particularly simple form, the assumptions of an infinitely heavy nucleus and $q \gg \omega$ (electron energy loss) have been made. The longitudinal and transverse form factors, F_L and F_T, respectively, contain all the nuclear structure information and are functions only of q. Thus, by working at fixed q and ω, but varying the initial electron energy so that the scattering angle (θ) varies, one can reduce Eq. (1.1) to the form

$$y = mx + b , \quad (1.2)$$

where m and b are constants and $x = [\tfrac{1}{2} + \tan^2(\theta/2)]$. The slope of the straight line, Eq. (1.2), obtained by varying E_i, the initial energy of the electron, and θ (for fixed q), gives the contribution of the transverse form factor. The extrapolated y intercept for $x = 0$ gives the longitudinal form factor contribution. Deviations from the straight line would be evidence of non-negligible higher order processes (such as two photon exchange). A non-zero longitudinal form factor contribution is evidence that a natural parity non-spin-flip transition is involved: $\Delta T = 0$ or 1 states being equally probable from an investigation of the transition operator alone. A zero contribution from the longitudinal form factor and an appreciable transverse form factor contribution most often indicate an unnatural parity spin-flip transition. Starting from a $T = 0$ target, such final states usually are assumed to have $T_f = 1$ because of the strong dominance of the isovector magnetic moment term in the transverse form factor.

Initially it may seem unlikely that such an approach can be used for pion-nucleus inelastic scattering, which at medium energies is certainly not dominated by a single real pion absorption and subsequent reemission. However, using the DWIA and fixed scatterer phase shifts, it is possible to obtain a simple expression for the energy and angle dependence of fixed momentum transfer pion-nucleus inelastic scattering. We will demonstrate that extra energy dependences associated with projectile absorption and variations of the elementary amplitude affect most states equivalently and thus effectively disappear in ratios of data. We also find that including such complications in model calculations often results in their effectively canceling each other.

In Sec. II we discuss the formulas and assumptions used to obtain our basic expression. The result can be applied to test whether a state is excited by the DWIA reaction mechanism and to determine the amounts of spin-flip involved in the excitation process. Other contributions to the reaction mechanism can be separated also. Various corrections to the basic formulas are discussed and estimated, and techniques for experimentally studying them are suggested. In Sec. III, the predictions of the fixed q, variable energy, and angle expression are compared with the experimental excitation functions for strongly excited states whose angular momentum and parity are well known. We find good agreement between theory and experiment, suggesting that our basic expression can be used with some confidence in the future, both in reaction-mechanism studies and for determining the spin-flip character of final nuclear states reached in (π, π'). We also present results showing the energy and state dependence of various terms entering in the basic formula. Some differential cross sections obtained using the formulas put forth in this paper are compared to those obtained using a more complete (but perhaps less instructive) momentum-space, finite-range DWIA code. In addition, we suggest future experiments of possible interest and make some predictions based on the formulas obtained in Sec. II. In Sec. IV, we briefly state and discuss our conclusions.

II. BASIC FORMULAS AND PROCEDURES

A. Isolating the q, E, and θ dependences in the inelastic transition amplitude

The differential cross section for pion induced excitation of an infinitely heavy nucleus from the initial state $|i\rangle$ to the final state $|f\rangle$ can be written as

$$\frac{d\sigma}{d\Omega} {}^{fi}_{\phi'_z, z} (\vec{k}', \vec{k}) = \frac{E(k')k'}{E(k)k} \, e^{q^2 b^2/2A}$$
$$\times \, |\langle f | \hat{F}_{\phi'_z, \phi_z} (\vec{k}', \vec{k}) |i\rangle|^2 , \quad (2.1)$$

where ϕ_z (ϕ'_z) denotes the pion's initial (final) charge and $\vec{k}$ ($\vec{k}'$) denotes the pion's initial (final) momentum. We adopt the convention of natural units ($\hbar = c = 1$) and use free particle relativistic kinematics for the pion, where $E^2(k) = k^2 + m_\pi^2$. The exponential function of momentum transfer, $\vec{q} = \vec{k}' - \vec{k}$, is the approximate center-of-mass correction for using harmonic oscillator shell-model wave functions, where b is the oscillator parameter and A is the atomic number. In general, the pion-nucleus transition operator $\hat{F}$ is a many-body operator on the space of target nucleons. Our major assumption in this work is that the DWIA is an adequate description of the pion-nucleus interaction for intermediate-energy inelastic scattering. (Like the one photon exchange assumption in the electron scattering, one hopes to critically test the DWIA assumption by varying E and θ appropriately.) Within the DWIA, the

pion-nucleus amplitude may be written in configuration space as

$$\langle f|\hat{F}_{\phi'_z,\phi_z}(\vec{k}',\vec{k})|i\rangle^{\mathrm{DWIA}}$$

$$\simeq \int d\vec{r}'d\vec{r}\, \Psi^{(-)*}_{f,\phi'_z}(\vec{k}',\vec{r}')$$

$$\times \langle f|\hat{t}_{\phi'_z,\phi_z}(\vec{r}',\vec{r})|i\rangle \Psi^{(+)}_{i,\phi_z}(\vec{k},\vec{r}), \qquad (2.2a)$$

or in momentum space as

$$\langle f|\hat{F}_{\phi'_z,\phi_z}(\vec{k}',\vec{k})|i\rangle^{\mathrm{DWIA}}$$

$$\simeq \int d\vec{\kappa}'d\vec{\kappa}\, \Psi^{(-)*}_{f,\phi'_z}(\vec{k}',\kappa')$$

$$\times \langle f|\hat{t}_{\phi'_z,\phi_z}(\vec{\kappa}',\vec{\kappa})|i\rangle \Psi^{(+)}_{i,\phi_z}(\vec{k},\kappa), \qquad (2.2b)$$

where $\Psi^{(+)}_i$ $[\Psi^{(-)*}_f]$ denotes the initial (final) pion distorted wave function. Equations (2.2a) and (2.2b) are, or course, equivalent representations, but momentum space offers a flexibility for including the nonlocality of the pion-nucleon interaction.

For the single-nucleon operator $\hat{t}$ we adopt the nonlocal, separable fixed scatterer parametrization of Piepho and Walker,[8] which has been used to study elastic and inelastic pion-nucleus scattering.[9] In the fixed scatterer formalism, the transition operator is local in the nucleon configuration space coordinate, thus allowing us to write

$$\hat{t}_{\phi'_z,\phi_z}(\vec{\kappa}',\vec{\kappa})= \sum_{lm'm}\left(\frac{4\pi}{2l+1}\right)\{[A_l\delta_{\phi'_z\phi_z}\hat{\rho}(\vec{\kappa}'-\vec{\kappa})+ B_l\langle\phi'_z|\vec{\phi}|\phi_z\rangle\cdot\hat{\vec{\rho}}(\vec{\kappa}'-\vec{\kappa})]\delta_{m'm}$$

$$+ [C_l\delta_{\phi'_z\phi_z}\hat{\vec{\sigma}}(\vec{\kappa}'-\vec{\kappa})+ D_l\langle\phi'_z|\vec{\phi}|\phi_z\rangle\cdot\hat{\vec{\sigma}}(\vec{\kappa}'-\vec{\kappa})]\langle lm'|\vec{L}|lm\rangle\} Y_{lm'}(\Omega_{\kappa'})Y^*_{lm}(\Omega_\kappa), \qquad (2.3)$$

where $\vec{\phi}$ and $\vec{L}$ denote the pion isospin and angular momentum operators. Note that $\hat{\vec{\rho}}$ and $\hat{\vec{\sigma}}$ are isovector and vector-isovector operators on the nuclear space. The coefficients A, B, C, and D contain the energy-momentum dependence and are linear combinations of the off-shell fixed scatterer pion-nucleon amplitudes, f^κ_{lgj}. The specific relations are

$$3A_l=\{[l\alpha+ (l+ 1)\beta]+ 2[l\gamma+(l+ 1)\delta]\}\ ,$$

$$3B_l=\{-[l\alpha+ (l+ 1)\beta]+ [l\gamma+ (l+ 1)\delta]\}\ ,$$

$$3C_l=[-(\alpha-\beta) - 2(\gamma-\delta)]\ , \qquad (2.4)$$

$$3D_l=[(\alpha-\beta) - (\gamma-\delta)]\ ,$$

where

$$\alpha \equiv f^k_{\substack{T=1/2\\j=l-1/2}}(\kappa',\kappa),\quad \beta\equiv f^k_{\substack{T=1/2\\j=l+1/2}}(\kappa',\kappa),$$

$$\gamma \equiv f^k_{\substack{T=3/2\\j=l-1/2}}(\kappa',\kappa),\quad \delta \equiv f^k_{\substack{T=3/2\\j=l+1/2}}(\kappa',\kappa), \qquad (2.5)$$

and

$$f^k_{lgj}(\kappa',\kappa)= \frac{v_{lgj}(\kappa')v_{lgj}(\kappa)}{v_{lgj}{}^2(k)}\, f^k_{lgj}, \qquad (2.6)$$

$$f^k_{lgj}\equiv \frac{e^{i\delta_{lgj}}\sin\delta_{lgj}(k)}{k}\ .$$

For the reaction studies reported in this paper, we have used the separable fixed scatterer form factors ($v's$) and phase shifts obtained in Ref. 8. The isoscalar and isovector matter-density and spin-density operators are defined as follows:

$$\hat{\rho}(\vec{x})= \sum_{j=1}^A \delta(\vec{x}-\vec{r}_j),$$

$$\hat{\vec{\rho}}(\vec{x})= \sum_{j=1}^A \vec{\tau}(j)\delta(\vec{x}-\vec{r}_j),$$

$$\hat{\vec{\sigma}}(\vec{x})= \sum_{j=1}^A \vec{\sigma}(j)\,\delta(\vec{x}-\vec{r}_j), \qquad (2.7)$$

$$\hat{\vec{\sigma}}(\vec{x})= \sum_{j=1}^A \vec{\tau}(j)\vec{\sigma}(j)\,\delta(\vec{x}-\vec{r}_j),$$

in terms of the nucleon Pauli spin ($\vec{\sigma}$) and the isospin ($\vec{\tau}$) operators. The Fourier transforms of Eqs. (2.7) have been used in Eq. (2.3); for example,

$$\hat{\rho}(\vec{\kappa}'-\vec{\kappa})= \int d\vec{x}\, e^{-i\vec{x}\cdot(\vec{\kappa}'-\vec{\kappa})}\hat{\rho}(\vec{x}). \qquad (2.8)$$

In order to obtain an expression analogous to Eq. (1.1), it is useful to treat the pion-nucleon coupling as a zero-range interaction and to adopt eikonal distorted waves, without Coulomb distortions. The adequacy of these approximations will be discussed in Sec. IIB. The zero-range approximation, including S-wave and P-wave channels, enables us to rewrite Eq. (2.3) (now also as an operator on the pion's isospin) as

$$\hat{t}(\vec{\kappa}',\vec{\kappa})=\bar{A}_0\,\hat{\rho}(\vec{\kappa}'-\vec{\kappa})+ \bar{B}_0\vec{\phi}\cdot\hat{\vec{\rho}}(\vec{\kappa}'-\vec{\kappa})$$

$$+ \frac{1}{k^2}[\bar{A}_1\hat{\rho}(\vec{\kappa}'-\vec{\kappa})+ \bar{B}_1\vec{\phi}\cdot\hat{\vec{\rho}}(\vec{\kappa}'-\vec{\kappa})]\vec{\kappa}\cdot\vec{\kappa}'$$

$$+ \frac{i}{k^2}[\bar{C}_1\hat{\vec{\sigma}}(\vec{\kappa}'-\vec{\kappa})+ \bar{D}_1\vec{\phi}\cdot\hat{\vec{\sigma}}(\vec{\kappa}'-\kappa)]\cdot(\vec{\kappa}\times\vec{\kappa}'). \qquad (2.9)$$

The barred quantities appearing in Eq. (2.9) are

obtained from the corresponding unbarred quantities defined in Eqs. (2.4)–(2.6) by letting $f_l^k(\kappa', \kappa)$ $\rightarrow (\kappa'/\kappa)^l f_l^k$. A more convenient representation of $\hat{t}$ for our purposes is the configuration-space representation of Eq. (2.9) given by

$$\hat{t}(\vec{r}', \vec{r}) = (2\pi)^3 \, \delta(\vec{r}'-\vec{r}) \, \{\bar{A}_0 \hat{\rho}(\vec{r}) + \bar{B}_0 \, \hat{\phi} \cdot \hat{\rho}(\vec{r})$$

$$+ \frac{1}{k^2} [\bar{A}_1 \hat{\rho}(\vec{r}) + \bar{B}_1 \hat{\phi} \cdot \hat{\rho}(\vec{r})] \, \nabla_r \cdot \nabla_{r'}$$

$$+ \frac{i}{k^2} [\bar{C}_1 \hat{\sigma}(\vec{r}) + \bar{D}_1 \, \hat{\phi} \cdot \hat{\sigma}(\vec{r})] \cdot \nabla_r$$

$$\times \nabla_{r'}\}, \tag{2.10}$$

where ∇_r operates on the incoming pion distorted wave and $\nabla_{r'}$ operates on the outgoing wave.

Using configuration-space eikonal distorted waves allows us to write

$$\Psi_i^{(+)}(\vec{k}, \vec{r}) \simeq \frac{e^{i\vec{k}\cdot\vec{r}}}{(2\pi)^{3/2}} \, e^{i\Delta\phi_i^{(+)}(\vec{r})} \tag{2.11a}$$

and

$$\Psi_f^{(-)}(\vec{k}', \vec{r}) \simeq \frac{e^{-i\vec{k}'\cdot\vec{r}'}}{(2\pi)^{3/2}} \, e^{i\Delta\phi_f^{(-)}(\vec{r}')}, \tag{2.11b}$$

where the nuclear medium modifies the plane waves through the complex "indices of refraction" $\Delta\phi_i$ and $\Delta\phi_f$ determined from optical potentials integrated along classical trajectories, that is,

$$\Delta\phi_i^{(+)}(\vec{r}) = -\frac{1}{2k} \int_{-\infty}^{\vec{r}} dz \, U_E(\vec{x}) \tag{2.12a}$$

and

$$\Delta\phi_f^{(-)*}(\vec{r}) = -\frac{1}{2k'} \int_{\vec{r}}^{\infty} dz' U_E'(\vec{x}). \tag{2.12b}$$

Inserting Eqs. (2.11a) and (2.11b) into Eq. (2.2a) and keeping terms of lowest order in the nuclear density one obtains

$$\langle f | \hat{F}_{\phi_z,\phi_z}(\vec{k}',\vec{k}) |i\rangle \simeq \langle f | \hat{\rho}_{\phi_z,\phi_z}^0(\vec{q}, E)\frac{\vec{k}\cdot\vec{k}'}{k^2} + i\hat{\sigma}_{\phi_z,\phi_z}(\vec{q}, E)\frac{\vec{k}\times\vec{k}'}{k^2} |i\rangle, \tag{2.13}$$

where

$$\hat{\rho}_{\phi_z,\phi_z}^i(\vec{q}, E) = \int d\vec{r} \, e^{-\vec{q}\cdot\vec{r}}[\bar{A}_i\delta_{\phi_z,\phi_z}\hat{\rho}(\vec{r}) + \bar{B}_i\langle\phi_z'|\hat{\phi}|\phi_z\rangle\cdot\hat{\rho}(\vec{r})]e^{iX(\vec{r}, E)} \tag{2.14}$$

and

$$\hat{\sigma}_{\phi_z,\phi_z}(\vec{q}, E) = \int d\vec{r} \, e^{-i\vec{q}\cdot\vec{r}} [\bar{C}_1\delta_{\phi_z,\phi_z}\hat{\sigma}(\vec{r}) + \bar{D}_1\langle\phi_z'|\hat{\phi}|\phi_z\rangle\cdot\hat{\sigma}(\vec{r})]e^{iX(\vec{r}, E)}. \tag{2.15}$$

The phase function $\chi \equiv \Delta\phi^{(+)} + \Delta\phi^{(-)*}$ represents the effect of the medium upon the incoming and outgoing pion waves. By using the standard approximation that the nuclear matter density is essentially the same in the initial and final channel and that $k' \simeq k$ in the phase factor, we may relate χ to the elastic scattering optical potential in the usual manner.

We now proceed to express the matter-density and spin-density operators of Eqs. (2.14) and (2.15) in terms of irreducible tensor operators. For the matter-density operator, we use the expansion

$$e^{-i\vec{q}\cdot\vec{r}} = 4\pi \sum_{J, M} (-i)^J j_J(qr) \, Y_{JM}(\Omega_r) \, Y_{JM}^*(\Omega_q) \tag{2.16}$$

to write Eq. (2.14) as

$$\hat{\rho}_{\phi_z,\phi_z}^i(\vec{q}, E) = 4\pi \sum_{J, M} (-i)^J \hat{M}_{JM}^i(q, E) \, Y_{JM}^*(\Omega_q), \tag{2.17}$$

where

$$\hat{M}_{JM}^i(q, E) = \int d\vec{r} \, e^{iX(\vec{r}, E)} j_J(qr) \, Y_{JM}(\Omega_r)$$

$$\times [\bar{A}_i\delta_{\phi_z,\phi_z}\hat{\rho}(\vec{r}) + \bar{B}_i\langle\phi_z'|\hat{\phi}|\phi_z\rangle\cdot\hat{\rho}(\vec{r})] \tag{2.18}$$

is an irreducible tensor operator on the nuclear Hilbert space.

The discussion for the spin-density operator is slightly more involved. First we define the basis of unit vectors with respect to $\vec{q}$,

$$\vec{e}_{q0} \equiv \frac{\vec{q}}{q}, \quad \vec{e}_{q\pm1} \equiv \mp\frac{1}{\sqrt{2}} (\vec{e}_x \pm i\vec{e}_y), \tag{2.19}$$

and note that

$$\vec{k}\times\vec{k}'\cdot\vec{\sigma} = \sum_{\lambda=\pm1} (\vec{k}\times\vec{k}')_\lambda^* \sigma_\lambda. \tag{2.20}$$

Next we use the identity for $\lambda = \pm1$

$$\vec{e}_{q\lambda} e^{-i\vec{q}\cdot\vec{r}} \equiv -\sqrt{2\pi} \sum_{J\geq1} (-i)^J J \{\lambda j_J(qr)\vec{Y}_{JJ1}^\lambda - q^{-1}\nabla$$

$$\times [j_J(qr)\vec{Y}_{JJ1}^\lambda]\}, \tag{2.21}$$

where

$$\vec{Y}_{JJ1}^\lambda \equiv (-)^{J-1-\lambda} \bar{J} \sum_{m,m} \begin{pmatrix} J & 1 & J \\ m & m' & \lambda \end{pmatrix} Y_{Jm}(\Omega_r)\vec{e}_{m'}. \tag{2.22}$$

are the vector spherical harmonics and we are using the notation $\bar{J} \equiv (2J+1)^{1/2}$. We may now write, using Eqs. (2.20) and (2.21),

$$\hat{\sigma}_\lambda = \sqrt{2\pi} \sum_{J \geq 1} (-i)^J \hat{J} [\hat{S}^u_{J\lambda} - \lambda \hat{S}^n_{J\lambda}], \qquad (2.23)$$

where

$$\hat{S}^n_{J\lambda}(q,E) \equiv \int d\vec{r}\, e^{iX(\vec{r},E)} j_J(qr) \vec{Y}^\lambda_{JJ1}$$
$$\cdot [\overline{C}_1 \delta_{\phi'_z,\phi_z} \vec{\hat{\sigma}}(\vec{r}) + \overline{D}_1 \langle \phi'_z | \vec{\Phi}_z | \phi_z \rangle \cdot \hat{\vec{\sigma}}(\vec{r})] \qquad (2.24)$$

and

$$\hat{S}^u_{J\lambda}(q,E) \equiv q^{-1} \int d\vec{r}\, e^{iX(\vec{r},E)} [\vec{\nabla} \times j_J(qr)\vec{Y}^\lambda_{JJ1}]$$
$$\cdot [\overline{C}_1 \delta_{\phi'_z,\phi_z} \vec{\hat{\sigma}}(\vec{r}) + \overline{D}_1 \langle \phi'_z | \vec{\Phi} | \phi_z \rangle \cdot \hat{\vec{\sigma}}(\vec{r})]. \qquad (2.25)$$

These operators are irreducible tensor operators on the space of nuclear states. In addition, $\hat{S}^n$ (natural) and $\hat{S}^u$ (unnatural) have opposite parity. We now apply the Wigner-Eckart theorem and obtain the basic result for unpolarized pion-nucleus inelastic scattering:

$$(2J_i+1)^{-1} \sum_{M_f,M_i} |\langle f | \hat{F}_{\phi'_z,\phi_z}(\vec{k},\vec{k}) | i \rangle|^2$$
$$= \frac{4\pi}{2J_i+1} \Big[F_{\rho 0}{}^2 + \cos(\theta) 2\,\mathrm{Re}\{F_{\rho 0} F^*_{\rho 1}\}$$
$$+ \cos^2(\theta) F_{\rho 1}{}^2 + \frac{\sin^2(\theta)}{2} F_\sigma{}^2 \Big], \qquad (2.26)$$

where

$$F_{\rho i}{}^2 = \left(\frac{k'}{k}\right)^{2i} \sum_{J=0}^\infty |\langle J_f T_f T_{zf} | |\hat{M}^i_J(q,E)| | J_i T_i T_{zi}\rangle|^2, \qquad (2.27)$$

$$F_\sigma{}^2 = \left(\frac{k'}{k}\right)^2 \sum_{J=1}^\infty \Big[|\langle J_f T_f T_{zf} | |\hat{S}^n_J(q,E)| | J_i T_i T_{zi}\rangle|^2$$
$$+ |\langle J_f T_f T_{zF} | |\hat{S}^u_J(q,E)| | J_i T_i T_{zi}\rangle|^2 \Big], \qquad (2.28)$$

and

$$\mathrm{Re}\{F_{\rho 0} F^*_{\rho 1}\} = \left(\frac{k'}{k}\right) \mathrm{Re}\left\{ \sum_{J=0}^\infty \langle J_f T_f T_{zf} | |M_J^0(q,E)| | J_i T_i T_{zi}\rangle \langle J_f T_f T_{zf} | |\hat{M}_J^1(q,E)| | J_i T_i T_{zi}\rangle^* \right\}. \qquad (2.29)$$

These results follow immediately from noting that by choosing $\vec{q}$ as the axis of quantization, $\hat{\rho}_i(q,E)[\hat{\sigma}(q,E)]$ carries angular momentum zero $[\pm 1]$ along $\vec{q}$ and thus ρ and σ cannot interfere in the sum over M_i and M_f because they lead to different final nuclear states. Using parity instead of angular momentum, a similar argument can be used for the noninterference of $\hat{S}^n$ and $\hat{S}^u$.[7]

To more fully understand the utility of Eq. (2.26), it is useful to extract the nuclear isospin T_z dependence and to relate the many-body reduced matrix elements to single-particle reduced matrix elements. One can use the Wigner-Eckart theorem to obtain reduced matrix elements in isospin space for Eqs. (2.27)–(2.29) yielding

$$\langle J_f T_f T_{zf} | |\hat{O}_{J;TT_z}| | J_i T_i T_{zi}\rangle$$
$$= (-)^{T_f - T_{zf}} \begin{pmatrix} T_f & T & T_i \\ -T_{zf} & T_z & T_{zi} \end{pmatrix} \langle J_f T_f \vdots \hat{O}_{JT} \vdots J_i T_i\rangle. \qquad (2.30)$$

Arbitrary many-body reduced matrix elements of a one-body operator may be written as sums of single-particle reduced matrix elements by using

$$\langle J_f T_f \vdots \hat{O}_{JT} \vdots J_i T_i\rangle = \sum_{\bar{\alpha},\bar{\beta}} \langle \bar{\alpha} \vdots \hat{O}_{JT} \vdots \bar{\beta}\rangle \xi^{fi}_{JT}(\bar{\alpha},\bar{\beta}), \qquad (2.31)$$

where

$$\xi^{fi}_{JT}(\bar{\alpha},\bar{\beta}) = \sum_{\substack{\text{over all} \\ z\text{ components}}} (-)^{J_f - M_f + j_\alpha - m_\alpha} \begin{pmatrix} J_f & J & J_i \\ -M_f & M & M_i \end{pmatrix} \begin{pmatrix} j_\alpha & J & j_\beta \\ -m_\alpha & M & m_\beta \end{pmatrix} (-)^{T_f - T_{zf} + 1/2 - t_\alpha} \begin{pmatrix} T_f & T & T_i \\ -T_{zf} & T_z & T_{zi} \end{pmatrix} \begin{pmatrix} \frac{1}{2} & T & \frac{1}{2} \\ -t_\alpha & T_z & t_\beta \end{pmatrix}$$
$$\times \xi^{(fi)}_{\alpha\beta}, \qquad (2.32)$$

and

$$\xi^{(fi)}_{\alpha\beta} \equiv \langle J_f M_f, T_f T_{zf} | c^\dagger_\alpha c_\beta | J_i M_i, T_i T_{zi}\rangle. \qquad (2.33)$$

The $c^\dagger_\alpha (c_\beta)$ appearing in Eq. (2.33) are second quantized creation (destruction) operators for a nucleon in the single-particle orbital α (β). We are using the notation $\bar{\alpha}$ to omit the "magnetic" quantum numbers, i.e., $\{\bar{\alpha}\} = \{n_\alpha l_\alpha j_\alpha\}$. For definiteness, if the initial state is a $J = T = 0$ closed-shell nucleus, $|i\rangle = |C\rangle$, and the final nuclear state is a pure particle-hole state given by

$$|\overline{\alpha}(\overline{\beta})^{-1}: J_f M_f T_f T_{Zf}\rangle = \tilde{J}_f \tilde{T}_f \sum_{m_\alpha, m_\beta, t_\alpha, t_\beta} (-)^{j_\alpha - m_\alpha + 1/2 - t_\alpha} \begin{pmatrix} j_\alpha & j_\beta & J_f \\ m_\alpha & -m_\beta & -M_f \end{pmatrix} \begin{pmatrix} \frac{1}{2} & \frac{1}{2} & T_f \\ t_\alpha & -t_\beta & -T_{Zf} \end{pmatrix} c_\alpha^\dagger c_\beta |C\rangle, \tag{2.34}$$

then $\xi_{JT}^{f0}(\overline{\alpha},\overline{\beta}) = \delta_{J_f J} \delta_{T_f T}$. If the particle-hole state is a linear combination of configuration-mixed pure particle-hole states,

$$|J_f M_f; T_f T_{Zf}\rangle = \sum_{\alpha,\beta} \gamma_{\overline{\alpha},\overline{\beta}}^{J_f T_f} |\overline{\alpha}(\overline{\beta})^{-1}: J_f M_f T_f T_{Zf}\rangle, \tag{2.35}$$

then

$$\xi_{JT}^{f0}(\overline{\alpha},\overline{\beta}) = \gamma_{\overline{\alpha},\overline{\beta}}^{J_f T_f} \delta_{J_f J} \delta_{T_f T}. \tag{2.36}$$

Thus, if one adopts the DWIA, the task is reduced to evaluating single-particle matrix elements of the operators given in Eqs. (2.18), (2.24), and (2.25). The precise expressions obtained for these single-particle reduced matrix elements depends upon the nature of the phase function $\chi(\vec{r},E)$. Over the energy region of consideration ($100 \lesssim T_\pi \lesssim 300$ MeV), the real part of the phase function χ^R is much less important than the imaginary term χ^I. The net effect of χ^R in Eqs. (2.18), (2.24), and (2.25) is to slightly alter the free-space momentum transfer appearing in these equations. To demonstrate this, we first note that χ^R and $\partial^2\chi^R/\partial E^2$ vanish at a laboratory kinetic energy near 180 MeV. If we make a Taylor series expansion through second order of χ^R about that point (E_0), we get

$$\chi^R(\vec{r},E) \simeq (E - E_0)(1 - \vec{r}_0 \cdot \vec{\nabla})\frac{\partial}{\partial E}\chi^R \Big|_{\vec{r}_0, E_0} + (E - E_0)\vec{r} \cdot \vec{\nabla}\frac{\partial}{\partial E}\chi^R \Big|_{\vec{r}_0, E_0}, \tag{2.37}$$

The first term on the right hand side of Eq. (2.37) is independent of $\vec{r}$ and thus contributes an overall phase (which we shall omit). The second term is then the lowest order contribution of χ^R to the integrands of Eqs. (2.18), (2.24), and (2.25). By adding this term to $-\vec{q} \cdot \vec{r}$, we see that χ^R effectively changes the momentum transfer. The actual importance of (2.37) is very small, yielding less than a 10% change (increase at 120 MeV and decrease at 250 MeV) of the free-space value of q and will be ignored in the following. For the purposes of this paper, we simplify the remaining attenuation factor $\exp[-\chi^I(\vec{r},E)]$ by treating it as a scalar function of the radius. This approximation may be improved upon, for example, by adopting the technique of McCarthy and Pursey.[10] Such a correction, however, will not alter the structure of our basic result, Eq. (2.26). By adopting the above treatment of $\chi(\vec{r},E)$ and by using standard techniques,[7] we obtain

$$\langle J_f T_f T_{Zf} || \hat{M}_J^t(q,E) || J_i T_i T_{Zi}\rangle = (-)^J \frac{\tilde{J}}{\sqrt{2\pi}} \sum_{\overline{\alpha},\overline{\beta}} (-)^{1/2 + J\beta} \tilde{j}_\alpha \tilde{j}_\beta \tilde{l}_\alpha \tilde{l}_\beta \begin{pmatrix} l_\alpha & J & l_\beta \\ 0 & 0 & 0 \end{pmatrix} \begin{Bmatrix} l_\alpha & j_\alpha & \frac{1}{2} \\ j_\beta & l_\beta & J \end{Bmatrix} (\overline{\alpha}|j_J e^{-\chi}|\overline{\beta})$$

$$\times [\overline{A}_i I_{\phi_Z \phi_Z}^{T_f 0 T_i} \xi_{J0}^{fi}(\overline{\alpha},\overline{\beta}) + \overline{B}_i I_{\phi_Z \phi_Z}^{T_f 1 T_i} \xi_{J1}^{fi}(\overline{\alpha},\overline{\beta})], \tag{2.38a}$$

$$\langle J_f T_f T_{Zf} || \hat{S}_J^\eta(q,E) || J_i T_i T_{Zi}\rangle = \left(\frac{3}{\pi}\right)^{1/2} (\tilde{J})^2 \sum_{\overline{\alpha},\overline{\beta}} (-)^{l\alpha} \tilde{j}_\alpha \tilde{j}_\beta \tilde{l}_\alpha \tilde{l}_\beta \begin{pmatrix} l_\alpha & J & l_\beta \\ 0 & 0 & 0 \end{pmatrix} \begin{Bmatrix} l_\alpha & \frac{1}{2} & j_\alpha \\ l_\beta & \frac{1}{2} & j_\beta \\ J & 1 & J \end{Bmatrix} (\overline{\alpha}|j_J e^{-\chi}|\overline{\beta})$$

$$\times [\overline{C}_1 I_{\phi_Z \phi_Z}^{T_f 0 T_i} \xi_{J0}^{fi}(\overline{\alpha},\overline{\beta}) + \overline{D}_1 I_{\phi_Z \phi_Z}^{T_f 1 T_i} \xi_{J1}^{fi}(\overline{\alpha},\overline{\beta})], \tag{2.38b}$$

$$\langle J_f T_f T_{Zf} || \hat{S}_J^u(q,E) || J_i T_i T_{Zi}\rangle = i\left(\frac{3}{\pi}\right)^{1/2} \sum_{\overline{\alpha},\beta} (-)^{l\alpha} \tilde{j}_\alpha \tilde{j}_\beta \tilde{l}_\alpha \tilde{l}_\beta$$

$$\times \sum_L [(J+1)^{1/2}\delta_{L,J-1} - \sqrt{J}\delta_{L,J+1}]\tilde{L} \begin{pmatrix} l_\alpha & L & l_\beta \\ 0 & 0 & 0 \end{pmatrix} \begin{Bmatrix} l_\alpha & \frac{1}{2} & j_\alpha \\ l_\beta & \frac{1}{2} & j_\beta \\ L & 1 & J \end{Bmatrix}$$

$$\times (\overline{\alpha}|j_L e^{-\chi}|\overline{\beta})[\overline{C}_1 I_{\phi_Z \phi_Z}^{T_f 0 T_i} \xi_{J0}^{fi}(\overline{\alpha},\overline{\beta}) + \overline{D}_1 I_{\phi_Z \phi_Z}^{T_f 1 T_i} \xi_{J1}^{fi}(\overline{\alpha},\overline{\beta})], \tag{2.38c}$$

where the isospin quantities are defined as

$$I_{\Phi'_Z \Phi_Z}^{T_f 0 T_i} \equiv \delta_{\Phi'_Z, \Phi_Z} \delta_{T_f, T_i} \delta_{T_{Zf}, T_{Zi}} (\bar{T}_i)^{-1}, \qquad (2.39a)$$

$$I_{\Phi'_Z \Phi_Z}^{T_f 1 T_i} \equiv 3\sqrt{2}(-)^{1-\Phi'_Z+T_f-T_{Zf}} \sum_{j=\pm 1,0} (-)^j \begin{pmatrix} 1 & 1 & 1 \\ -\phi'_Z & -j & \phi_Z \end{pmatrix}$$

$$\times \begin{pmatrix} T_f & 1 & T_i \\ -T_{Zf} & j & T_{Zi} \end{pmatrix}, \qquad (2.39b)$$

and the radial integrals are defined by

$$(\bar{\alpha} | j_L e^{-\chi} | \bar{\beta}) \equiv \int_0^\infty dr\, r^2 R_\alpha(r) j_L(qr) e^{-\chi^I(r,E)} R_\beta(r). \qquad (2.40)$$

In addition to the above results, there are several correction factors that we include and discuss in Sec. II C which complicate Eq. (2.26), etc., slightly. However, because the features of the basic formula survive in most cases, we outline in the next subsection some suggestions for using Eq. (2.26) to separate various contributions to the inelastic scattering and study different "types" of nuclear states. The opportunities associated with studies involving correction terms of potential importance are discussed in Sec. II C.

B. Utilization of the explicit q, E, and θ dependences

Using the results of Sec. II A, the differential cross section for inelastic pion scattering to a particular final nuclear state can be written schematically as

$$\frac{d\sigma}{d\Omega}(q,E,\theta) = \left[\frac{E(k')k'}{E(k)k}\right]\left[\left|\bar{A}_0(E) + \left(\frac{k'}{k}\right)\bar{A}_1(E)\cos\theta\right|^2 \mathfrak{M}^2(q,E)\right.$$

$$\left. + \left(\frac{k'}{k}\right)^2 |\bar{C}_1(E)|^2 \sin^2\theta\, \mathfrak{S}^2(q,E)\right], \qquad (2.41)$$

where we have assumed an isoscalar transition. An analogous expression, with $\bar{B}(E)$ and $\bar{D}(E)$ substituted for $\bar{A}(E)$ and $\bar{C}(E)$, exists for isovector transitions. In Eq. (2.41) the symbols $\bar{A}$ and $\bar{B}$ contain the energy dependence associated with the elementary fixed scatterer pion-nucleon amplitudes. The form factors $\mathfrak{M}$ and $\mathfrak{S}$ contain the distorted wave attenuation factor $\exp[-\chi^I(r,E)]$ and are thus energy dependent, unlike the situation for no distortions. However, we find the energy dependence of $\mathfrak{M}$ and $\mathfrak{S}$ to be very similar for values of q (denoted by q_{max}) for which the form factors are at a maximum. We also note that, in general, only the $\mathfrak{S}$ form factor contributes to unnatural parity transitions whereas both $\mathfrak{M}$ and

$\mathfrak{S}$ contribute to natural parity transitions. In the following discussion we suggest several ways of using Eq. (2.41).

1. Fixed q plots varying E and θ

Over the medium-energy range, the pion-nucleon interaction is dominated by the P_{33} partial wave. If we keep only this part of the pion-nucleon amplitude, Eq. (2.41) becomes

$$\frac{d\sigma}{d\Omega}(q,E,\theta) = \left[\frac{E(k')k'}{E(k)k}\right]\left(\frac{k'}{k}\right)^2 |\tfrac{2}{3} f_{33}^k|^2$$

$$\times [4\mathfrak{M}^2(q,E)\cos^2\theta + \mathfrak{S}^2(q,E)\sin^2\theta], \qquad (2.42)$$

which results from $\bar{A}_1 = 2\bar{C}_1 = (\tfrac{4}{3})f_{33}$ in the limit of P_{33} dominance [cf, Eq. (2.4)]. By equating the energy dependence of $\mathfrak{M}$ and $\mathfrak{S}$ at fixed q_0 (near q_{max}), Eq. (2.42) gives us

$$\frac{d\sigma}{d\Omega}(q_0,E,\theta) = \Gamma(E)[4\mathfrak{M}^2(q_0)\cos^2\theta + \mathfrak{S}^2(q_0)\sin^2\theta]. \qquad (2.43)$$

At this point, we can easily obtain an expression analogous to the one used in electron scattering for making Rosenbluth plots. Namely, for values of $\theta < 90°$ we define

$$G(E,\theta) \equiv \frac{d\sigma}{d\Omega}(q_0,E,\theta)[\Gamma(E)\cos^2\theta]^{-1} \qquad (2.44)$$

and obtain from Eq. (2.43)

$$G(E,\theta) = 4\mathfrak{M}^2(q_0) + \mathfrak{S}^2(q_0)\tan^2\theta, \qquad (2.45)$$

which is of the form $y = mx + b$, with $x = \tan^2\theta$. Thus, the slope of a plot of Eq. (2.45) as a function of $\tan^2\theta$ would yield the contribution resulting from the P-wave spin-flip part of the pion-nucleon amplitude, and the x intercept would yield the spin-independent P-wave term. For an unnatural parity transition, we note that the intercept is zero. Equation (2.45) may be useful in determining the unknown parity of a given transition or component in a complex of states. Deviations from a straight line are evidence that the simple theory is breaking down. Detailed examples for known states where data is available are given in Sec. III. Equation (2.43) has been found to be reliable in predicting whether a given excited state of a $J = 0$ nucleus reached by pion inelastic scattering has natural or unnatural parity. Because of the different θ dependence involved, plots using Eq. (2.43) at fixed q as a function of E are quite different for natural and unnatural parity transitions, and some examples are shown in Sec. III. In these plots we use q_0^2 $= |\vec{k}' - \vec{k}|^2 = (k')^2 + (k)^2 - 2k'k\cos\theta$ to determine θ

as a function of the incident pion energy $E(k)$, given the fixed momentum transfer q_0 and energy loss $E(k) - E(k')$.

For natural parity states there is an angle-independent term associated with the S-wave contribution to the transition operator [see Eq. (2.47)]. After using Eqs. (2.43) and (2.45) to establish that a given state does result from a natural parity transition, one may then wish to separate the S-wave and P-wave spin- and non-spin-slip contributions to the reaction. If a normal parity transition results from the promotion of a single nucleon from a particular initial orbital to a particular final orbital (for example $1p \rightarrow 1d$), one may show from Eq. (2.38) that $S_n{}^2(q, E)$ $= N \mathfrak{M}^2(q, E)$, where N is a constant. Now by defining the quantity

$$\mathcal{G}(E, \theta) \equiv \frac{d\sigma}{d\Omega} (q, E, \theta) \left\{ \left[\frac{E(k')k'}{E(k)k} \right] \mathfrak{M}^2(q, E) \right\}^{-1},$$

(2.46)

one can obtain from Eq. (2.41) the result

$$\mathcal{G}(E, \theta) = \left| \bar{A}_0(E) + \left(\frac{k'}{k} \right) \bar{A}_1(E) \cos\theta \right|^2$$

$$+ \left| N \left(\frac{k'}{k} \right) \bar{C}_1(E) \right|^2 \sin^2\theta.$$

(2.47)

By working at $\theta = 90°$, one may isolate the S-wave and P-wave spin-flip contributions. Also by looking at small angles only the S-wave and P-wave non-spin-flip survive. Because this can be done at the same energy, separation of these components is possible in principle. Note that the separation is *not* model independent, because a model of the form factor $\mathfrak{M}(q, E)$ is required. Nonetheless, Eq. (2.47) allows one to carry out self-consistent studies within a given model to isolate various reaction contributions.

2. Energy dependence of angle-integrated cross sections

There are circumstances, such as in activation experiments, where one may be interested in the angle-integrated differential cross section for a particular transition,

$$\sigma_{fi}(E) = 2\pi \int_0^\pi \frac{d\sigma^{fi}}{d\Omega} (q, E, \theta) \sin\theta \, d\theta.$$

(2.48)

At each value of E, q is a function of θ (or equivalently, θ is a function of q), so that σ_{fi} depends only on E. Because we have written the nuclear form factors $\mathfrak{M}$ and S in Eq. (2.41) as functions of q, we will change the integration variable in Eq. (2.48) from θ to q. For the purpose of this

discussion it will suffice to take $k' \simeq k$. Then from the relation $q^2 \simeq 2 k^2 (1 - \cos\theta)$, we get $\sin\theta \, d\theta \simeq k^{-2} q \, dq$, and by inserting Eq. (2.41) into Eq. (2.48), we obtain

$$\sigma_{fi}(E) \simeq \frac{2\pi}{k^2} \int_0^{4k^2} \left[\left| \bar{A}_0(E) + \left(1 - \frac{q^2}{2k^2} \right) \bar{A}_1(E) \right|^2 q \mathfrak{M}^2(q, E) \right.$$

$$+ \left. \frac{|\bar{C}_1(E)|^2}{k^2} \left(1 - \frac{q^2}{4k^2} \right) q^2 S^2(q, E) \right] dq.$$

(2.49)

From this expression, we observe the following qualitative predictions.

Because the nuclear form factors $\mathfrak{M}$ and S usually peak at small to moderate values of q, Eq. (2.49) implies that as the energy increases, the P-wave non-spin-flip contribution to a natural parity transition would generally dominate the spin-flip contribution. Similarly, as the energy increases, angle-integrated differential cross sections for natural parity transitions would dominate those for unnatural parity transitions. In summary, the different behavior is expected because as the energy increases, the nuclear form factor is concentrated at smaller angles and natural (unnatural) parity transitions contain an additional $\cos^2\theta$ ($\sin^2\theta$) term in the integrand that tends to increase (decrease) the integrated inelastic cross sections.

C. Fermi-motion corrections

There are, of course, several corrections to the approximations we have used in obtaining our basic results for pion-nucleus inelastic scattering [Eqs. (2.26)–(2.29)]. For example, using fixed scatterer phase shifts to incorporate the two-body input into the many-body problem is not a unique procedure.[11] Certainly, one must use some technique for transforming the two-body angular dependence into the many-body system. Our experience has been that most techniques give similar results, except at angles $\gtrsim 120°$ (where many other "higher order" effects may be important), and the fixed scatter approach is a reasonable method of carrying out this transformation.[12] The question of at what energy and momentum to evaluate the two-body input has also received considerable attention. A definite answer would require a more complete theory of the pion-nucleon interaction. However, one may phrase the question in terms of the total energy available in the off-shell pion-nucleon system, or the relative pion-nucleon momentum. And in principle, one might argue that energy-dependent studies at fixed momentum transfer would be useful in distinguishing between different models. The

practical difficulty at present is that there are several possible changes (arising from local field corrections, or alternatively stated, from isobar interactions in the medium) that have not been theoretically studied for inelastic scattering, and therefore their predicted effects are not known. This is important work for the future. One important correction that can be easily studied in the present context is the effect of the Fermi motion of the target nucleons. In the following, we include the effects of Fermi motion by generalizing a discussion originally given by Wilkin.[13]

The pion-nucleon transition operator may be considered, in general, as a function of the square of the invariant energy (s) and momentum transfer. Because the pion-nucleon interaction is a rapidly varying function of energy, we will consider only corrections that result from the energy variation. The fixed scatterer pion-nucleon transition operator given by Eq. (2.10) has been evaluated for the case of $\vec{p}$ (initial nucleon's momentum) $= \vec{p}'$ (final nucleon's momentum) $= 0$. If we denote the fixed scatterer value of the invariant energy by s_0, we can obtain an expression for the pion-nucleon transition operator that allows for nucleon motion by making a Taylor series expansion about s_0.

Let us consider the energy-dependent coefficients of the non-spin-flip part of the interaction. For the isoscalar term we obtain

$$\overline{A}_I(s) = \overline{A}_I(s_0) + (s - s_0)\frac{\partial}{\partial s}\overline{A}_I\Big|_{s_0}$$

$$+ \frac{(s - s_0)^2}{2}\frac{\partial}{\partial s^2}\overline{A}_I\Big|_{s_0} + \cdots . \qquad (2.50)$$

An analogous expression exists for the isovector term. Numerical estimates indicate that in the medium-energy region, the dominant correction is given by the first-derivative term of Eq. (2.50). By using the approximate relationships

$$s \simeq s_0 - (\vec{k} + \vec{k}') \cdot \frac{(\vec{p} + \vec{p}')}{2} \qquad (2.51)$$

and

$$\frac{\partial}{\partial s} \simeq \left(\frac{1}{2m_N}\right)\frac{\partial}{\partial E}, \qquad (2.52)$$

we obtain Fermi-motion corrections to the non-spin-flip part of the fixed scatterer pion-nucleon transition operator by replacing in Eq. (2.10) $\overline{A}_I\hat{\rho}$ by $(\overline{A}_I\hat{\rho})'$ and $\overline{B}_I\hat{\rho}$ by $(\overline{B}_I\hat{\rho})'$, where

$$[\overline{A}_I\hat{\rho}(\vec{r})]' = \overline{A}_I\hat{\rho}(\vec{r}) - \left(\frac{\partial\overline{A}_I}{\partial E}\right)\frac{(\vec{k}+\vec{k}')}{2}\cdot\hat{\vec{j}}_N(\vec{r})$$

$$(2.53a)$$

and

$$[\overline{B}_I\hat{\rho}(\vec{r})]' = \overline{B}_I\hat{\rho}(\vec{r}) - \left(\frac{\partial\overline{B}_I}{\partial E}\right)\frac{(\vec{k}+\vec{k}')}{2}\cdot\hat{\vec{j}}_N(\vec{r}).$$

$$(2.53b)$$

The nuclear current-density operators appearing in Eq. (2.53) are defined as

$$\hat{\vec{j}}_N(\vec{r}) = \sum_{j=1}^{A}\left(\frac{1}{im_N}\right)[\delta(\vec{r}-\vec{r}_j)\vec{\nabla}(j)]_{\text{sym}}$$

and

$$\hat{\vec{j}}_N(\vec{r}) = \sum_{j=1}^{A}\left[\frac{\vec{\tau}(j)}{im_N}\right][\delta(\vec{r}-\vec{r}_j)\vec{\nabla}(j)]_{\text{sym}}, \qquad (2.54)$$

where $[AB]_{\text{sym}} \equiv (AB + BA)/2$.

One of the most important implications of these correction terms is that they allow the relatively large non-spin-flip part of the pion-nucleon interaction to contribute to unnatural parity (spin-flip) transitions (as Wilkin has previously discussed for pion charge-exchange reactions at low q). This can be seen by noting that the correction terms are in the form of a pionic current coupling to the nuclear convection current. Just as the coupling of the electron current to the nuclear convection current contributes to both the transverse electric (natural parity transition) and transverse magnetic (unnatural parity transition) components of the transverse form factor in electron scattering, the Fermi-motion terms in Eq. (2.53) contribute to both natural parity and unnatural parity transitions. In the following, we will assume that the major effects of nucleon Fermi-motion can be incorporated by the substitutions given by Eq. (2.53).

Because of the vector nature of the Fermi-motion corrections, we include these terms by replacing in Eq. (2.13)

$$\frac{\vec{k}\times\vec{k}'}{k^2}\cdot\hat{\vec{\sigma}}_{\Phi_g,\Phi_g} \rightarrow \frac{\vec{k}\times\vec{k}'}{k^2}\cdot\hat{\vec{\sigma}}_{\Phi_g,\Phi_g} - \frac{(\vec{k}+\vec{k}')}{2i}\cdot\hat{\vec{j}}_{\Phi_g,\Phi_g}.$$

$$(2.55)$$

In analogy to the spin-density operator defined by Eq. (2.15), we have the current-density

$$\hat{\vec{j}}_{\Phi_g,\Phi_g} = \int d\vec{r}\, e^{-i\vec{q}\cdot\vec{r}}[\mathfrak{A}\delta_{\Phi_g,\Phi_g}\hat{\vec{j}}_N(\vec{r}) + \mathfrak{B}\langle\phi_g'|\vec{\phi}|\Phi_g\rangle\cdot\hat{\vec{j}}_N(\vec{r})]$$

$$\times e^{iX(\vec{r}, E)}, \qquad (2.56)$$

where

$$\mathfrak{A} \equiv \left(\frac{\partial\overline{A}_0}{\partial E}\right) + \left(\frac{\partial\overline{A}_1}{\partial E}\right)\left(\frac{k'}{k}\right)\cos\theta \qquad (2.57a)$$

and

$$\mathfrak{B} \equiv \left(\frac{\partial \overline{B}_0}{\partial E}\right) + \left(\frac{\partial \overline{B}_1}{\partial E}\right)\left(\frac{k'}{k}\right)\cos\theta . \qquad (2.57\text{b})$$

For all practical purposes we can ignore the S-wave derivatives in Eq. (2.57). See Fig. 2 for a comparison of S-wave to P-wave derivatives. Our developments now parallel those of the spin-density operator. We resolve $\vec{j}_{\phi_i,\phi_z}$ onto the basis given by Eq. (2.19), and in analogy with Eq. (2.20) we write

$$(\vec{k}+\vec{k}')\cdot\vec{j} = \sum_{\lambda=\pm1}(\vec{k}+\vec{k}')_\lambda^* j_\lambda . \qquad (2.58)$$

We note that on this basis

$$(\vec{k}\times\vec{k}')_\lambda^* = -\left(\frac{\lambda}{\sqrt{2}}\right)|\vec{k}\times\vec{k}'| \qquad (2.59)$$

and

$$(\vec{k}+\vec{k}')_\lambda^* = \left(\frac{i}{\sqrt{2}}\right)|\vec{k}+\vec{k}'| \qquad (2.60)$$

because $\vec{k}\times\vec{k}'$ is along the x axis, whereas $\vec{k}+\vec{k}'$ is along the y axis. By using the expansion given by Eq. (2.21), we obtain an expression analogous to Eq. (2.23),

$$j_\lambda = \sqrt{2\pi}\sum_{J>1}(-i)^J\tilde{J}\left(\hat{\mathfrak{g}}^n_{J\lambda} - \lambda\hat{\mathfrak{g}}^u_{J\lambda}\right), \qquad (2.61)$$

where $\hat{\mathfrak{g}}^n$ and $\hat{\mathfrak{g}}^u$ are defined by Eqs. (2.25) and (2.24), respectively, if we replace σ by j_N, $\overline{C}$ by $\mathfrak{C}$, and $\overline{D}$ by $\mathfrak{B}$ in those equations. Finally, by applying the Wigner-Eckart theorem and using the relation $|\vec{k}+\vec{k}'| \simeq \sqrt{kk'}\,2\cos(\theta/2)$, we arrive at the following expression for the nuclear current effects that must be added to our basic result [Eq. (2.26)] for unpolarized pion–nucleus inelastic scattering:

$$(2J_i+1)^{-1}\sum_{M_f,M_i}|F'|^2 = \frac{2\pi}{(2J_i+1)}\left[\cos^2(\theta/2)\cos^2\theta\, F_c^2 - \sin(2\theta)\cos(\theta/2)\,\text{Re}\{F_\sigma F_c^*\}\right], \qquad (2.62)$$

where

$$F_c^2 = (k')^2\left(\frac{k'}{k}\right)\sum_{J=1}^{\infty}\left[\,|\langle J_f\,T_f\,T_{zf}||\,\hat{\mathfrak{g}}^n_J\,||J_i\,T_i\,T_{zi}\rangle|^2 + |\langle J_f\,T_f\,T_{zf}||\,\hat{\mathfrak{g}}^u_J\,||J_i\,T_i\,T_{zi}\rangle|^2\right] \qquad (2.63)$$

and

$$\text{Re}\{F_\sigma F_c^*\} = k'\left(\frac{k'}{k}\right)^{3/2}\sum_{J=1}^{\infty}\text{Re}(\langle J_f\,T_f\,T_{zf}||\,\hat{S}^n_J\,||J_i\,T_i\,T_{zi}\rangle\langle J_f\,T_f\,T_{zf}||\,\hat{\mathfrak{g}}^n_J\,||J_i\,T_i\,T_{zi}\rangle^*$$
$$+ \langle J_f\,T_f\,T_{zf}||\,\hat{S}^u_J\,||J_i\,T_i\,T_{zi}\rangle\langle J_f\,T_f\,T_{zf}||\,\hat{\mathfrak{g}}^u_J\,||J_i\,T_i\,T_{zi}\rangle^*). \qquad (2.64)$$

The reduced matrix elements of the spin-density operators were given in Eq. (2.38). If we apply the same techniques used to obtain those results, we get for the reduced matrix elements of the current-density operators

$$\langle J_f\,T_f\,T_{zf}||\,\hat{\mathfrak{g}}^u_J\,||J_i\,T_i\,T_{zi}\rangle = \left(\frac{-i}{m_N}\right)\left(\frac{1}{2\pi}\right)^{1/2}(\tilde{J})^2\sum_{\bar{\alpha},\bar{\beta}}(-)^{l_\alpha+j_\beta-1/2}\,\tilde{j}_\alpha\tilde{j}_\beta\tilde{l}_\alpha(\tilde{l}_\beta)^{-1}\begin{Bmatrix}l_\alpha & j_\alpha & \frac{1}{2}\\ j_\beta & l_\beta & J\end{Bmatrix}\mathfrak{R}^{\alpha\beta}_{JJ}(q,E)$$

$$\times\left[\left(\frac{\partial\overline{A}_1}{\partial E}\right)I^{T_f 0 T_i}_{\Phi_z,\Phi_z}\,\xi^{f_i}_{J0}(\bar{\alpha},\bar{\beta}) + \left(\frac{\partial\overline{B}_1}{\partial E}\right)I^{T_f 1 T_i}_{\Phi_z,\Phi_z}\,\xi^{f_i}_{J1}(\bar{\alpha},\bar{\beta})\right] \qquad (2.65\text{a})$$

and

$$\langle J_f\,T_f\,T_{zf}||\,\hat{\mathfrak{g}}^n_J\,||J_i\,T_i\,T_{zi}\rangle = \left(\frac{1}{m_N}\right)\left(\frac{1}{2\pi}\right)^{1/2}\sum_{\bar{\alpha},\bar{\beta}}(-)^{l_\alpha+j_\beta-1/2}\,\tilde{j}_\alpha\tilde{j}_\beta\tilde{l}_\alpha(\tilde{l}_\beta)^{-1}$$

$$\times\begin{Bmatrix}l_\alpha & j_\alpha & \frac{1}{2}\\ j_\beta & l_\beta & J\end{Bmatrix}\sum_L[(J+1)^{1/2}\delta_{L,J-1} - \sqrt{J}\,\delta_{L,J+1}]\mathfrak{R}^{\alpha\beta}_{JL}(q,E)\tilde{L}$$

$$\times\left[\left(\frac{\partial\overline{A}_1}{\partial E}\right)I^{T_f 0 T_i}_{\Phi_z,\Phi_z}\,\xi^{f_i}_{J0}(\bar{\alpha},\bar{\beta}) + \left(\frac{\partial\overline{B}_1}{\partial E}\right)I^{T_f 1 T_i}_{\Phi_z,\Phi_z}\,\xi^{f_i}_{J1}(\bar{\alpha},\bar{\beta})\right], \qquad (2.65\text{b})$$

where

$$\mathcal{R}^{\alpha\beta}_{JL}(q,E) = \begin{Bmatrix} L & 1 & J \\ l_\beta & l_\alpha & l_\beta+1 \end{Bmatrix} \frac{\begin{pmatrix} l_\alpha & L & l_\beta+1 \\ 0 & 0 & 0 \end{pmatrix}}{\begin{pmatrix} l_\beta+1 & 1 & l_\beta \\ 0 & 0 & 0 \end{pmatrix}} (l_\beta+1)\left(\bar{\alpha}\left| e^{-x}j_L\left(\frac{d}{dr}-\frac{l_\beta}{r}\right)\right|\bar{\beta}\right)$$

$$+ \begin{Bmatrix} L & 1 & J \\ l_\beta & l_\alpha & l_\beta-1 \end{Bmatrix} \frac{\begin{pmatrix} l_\alpha & L & l_\beta-1 \\ 0 & 0 & 0 \end{pmatrix}}{\begin{pmatrix} l_\beta-1 & 1 & l_\beta \\ 0 & 0 & 0 \end{pmatrix}} (l_\beta)\left(\bar{\alpha}\left| e^{-x}j_L\left(\frac{d}{dr}+\frac{l_\beta+1}{r}\right)\right|\bar{\beta}\right). \tag{2.65c}$$

There are several points that we would like to note concerning the role of the Fermi-motion contributions given above as compared to our former result [Eq. (2.26)] without Fermi-motion effects. First, the current-density terms $(\hat{\jmath})$ do not interfere with the matter-density terms $(\hat{\rho}_i)$ for the same reason that the spin-density terms $(\hat{\sigma})$ could not interfere. [See the paragraph following Eq. (2.29).] However, the current-density terms do interfere with the spin-density terms and that effect is given by the $\mathrm{Re}\{F_\sigma F_c^*\}$ contribution to Eq. (2.62). This part of the differential cross section can change sign as a function of E, and therefore it should cause constructive and destructive interference with the zeroth-order terms depending on the energy of the pion. In addition, because of the θ-dependent factors, one may expect an angle dependence in the correction term, working at fixed q. An interesting and potentially useful point is that the nuclear-current correction term and the spin-dependent term have a different relative q dependence for pion inelastic scattering than the magnetization and convection current densities have in electron scattering. Also, we note that if one is considering a transition from a closed-shell nucleus to a particle-hole $1\hbar\omega$ "stretched" state [such as the $1f_{7/2}(1d_{5/2})^{-1}6^-$ state in ^{28}Si or the $1d_{5/2}(1p_{3/2})^{-1}4^-$ state in ^{16}O], the Fermi-motion correction term cannot contribute. This occurs because the ΔJ_{max} needed for a stretched-state transition is $\Delta J_{\mathrm{max}} = L_{\mathrm{max}}+1$, whereas the correction term can only provide a $\Delta J_{\mathrm{max}} = L_{\mathrm{max}}$ (for $L_{\mathrm{max}} = l_{\mathrm{particle}} + l_{\mathrm{hole}}$) because the correction term contains no spin dependence. (The situation in electron scattering is completely analogous. That is, the charge convection current also does not contribute to electroexcitation of stretched states.) Finally, we note that using "Fermi-averaged" values for $\bar{A}_i$ and $\bar{B}_i$ would only change the values of $\bar{A}_i$ and $\bar{B}_i$ inserted in $F_{\rho i}$ and would not lead to changes in F_σ. Thus it would not be inconsistent to use Fermi-averaged values and also include the correction terms for $\bar{A}_i$ and

$\bar{B}_i$ discussed above. The Fermi-averaged contributions can be thought of as resulting from terms in the Taylor series expansion other than the first-derivative term.

In summary, the contribution to unnatural parity states resulting from the non-spin-flip correction term should have a different effect (constructive versus destructive interference) above and below the $(3,3)$ resonance — except for stretched unnatural parity transitions, where it should have no effect. In the next section we shall study in detail the effect of the correction term for some specific example. In a future publication, we plan to expand and generalize the discussion presented here concerning nucleon motion correction terms.

III. NUMERICAL EXAMPLES

We devote this section to specific applications of some of the formulas derived in the previous section, so that we may underscore the main ideas discussed there. To perform numerical calculations, we need to specify the fixed scatterer pion-nucleon amplitudes, the distorted wave attenuation factor, and the structure of the specific nuclear state being considered. Because the pion-nucleon input is basic to all calculations and is not subject to further treatment, we will discuss it first.

A. The pion-nucleon fixed scatterer input

The pion-nucleon scattering amplitudes enter into our formulas through the coefficients $\bar{A}$, $\bar{B}$, $\bar{C}$, and $\bar{D}$. These coefficients are linear combinations of the fixed scatterer pion-nucleon scattering amplitudes. The particular linear combinations are given by Eq. (2.4). Using the fixed scatterer phase shifts of Ref. 8, we have constructed the S-wave and P-wave coefficients for medium energies and they are displayed in Fig. 1. As a consequence of the $(3,3)$ dominance over most of the medium energy region, the P-wave coefficients have the approximate relationship $\bar{A}_1 \simeq 2\bar{B}_1$
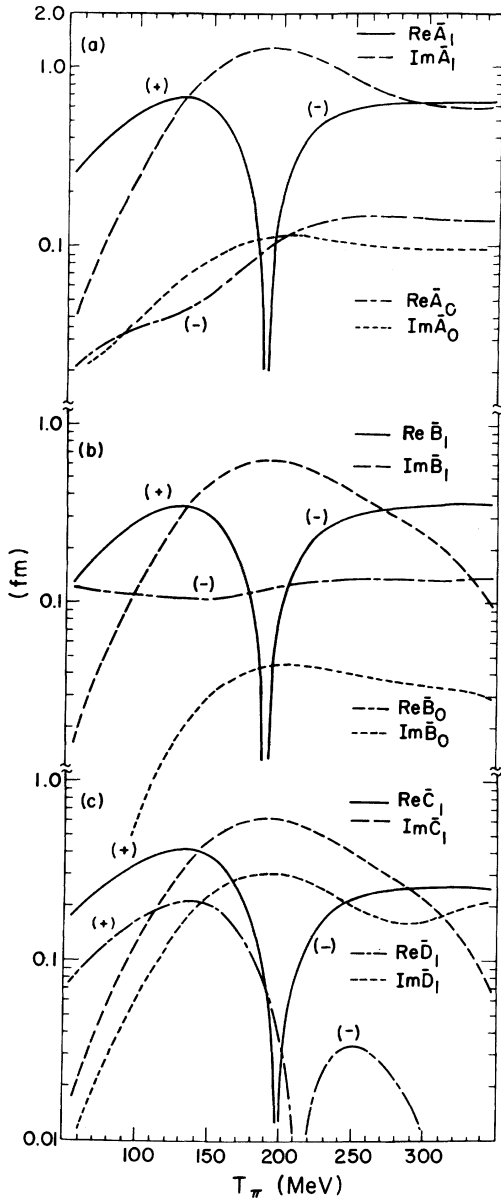
FIG. 1. The zero-range fixed scatterer pion-nucleon coefficients used as input for the EZRA calculations reported in this paper. All values are positive, except when otherwise indicated. (a) The S-wave and P-wave non-spin-flip isoscalar coefficients. Note that the real part of the S-wave coefficient is negative whereas the real part of the P-wave changes sign. (b) The S-wave and P-wave non-spin-flip isovector coefficients. Note the same behavior as in (a). (c) The P-wave spin-flip-isoscalar $(\bar{C}_1)$ and isovector $(\bar{D}_1)$ coefficients. Again note that the real parts change sign.

$\simeq 2\,\bar{C}_1 \simeq 4\,\bar{D}_1$. In Fig. 2 we display the derivatives with respect to energy of the S-wave and P-wave non-spin-flip coefficients. The Fermi-motion corrections discussed in Sec. II C depend upon
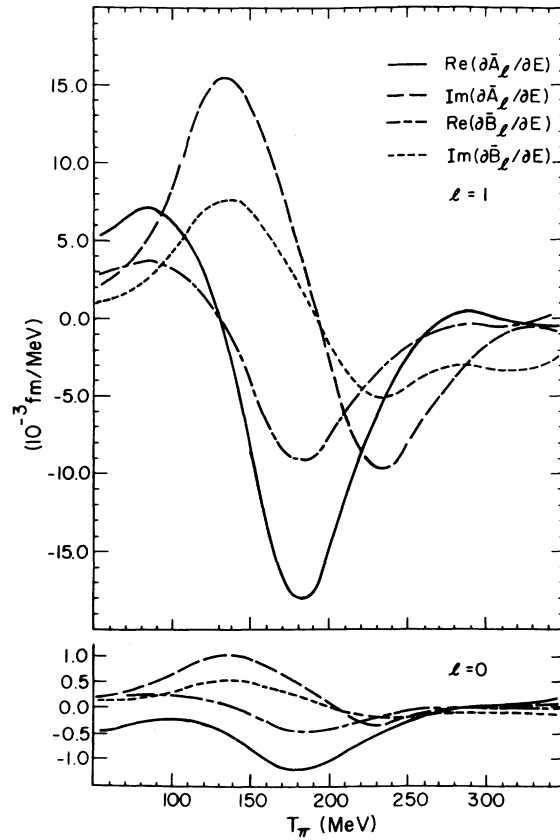

FIG. 2. The derivatives with respect to energy of the S-wave and P-wave non-spin-flip coefficients depicted in Fig. 1. These derivatives are used to calculate the Fermi-motion corrections presented in this paper.

these derivatives. Note, in Fig. 2, that the S-wave derivatives are negligible as compared to the P-wave derivatives.

B. Treatment of the distorted wave attenuation factor

The initial and final pion distorted waves enter our formulation through the eikonal phase factor $\chi(\vec{r}, E) = \Delta\phi^{(+)} + \Delta\phi^{(-)*}$, defined in Eq. (2.12). If, in our treatment of χ, we let the final nuclear density be the same as the initial density and $|\vec{k}'| \simeq |\vec{k}|$, we may relate χ to the optical potential U by the usual integration along the average of the initial and final momenta

$$\chi(\vec{r}, E) \simeq \left(\frac{-1}{2k}\right) \int_{-\infty}^{\infty} dz\, U_E(\vec{x}). \tag{3.1}$$

In principle, one should treat the phase function as carefully as possible, so as to reproduce the same results obtained by solving the corresponding Klein-Gordon equation.[14] For demonstrative purposes, however, we treat χ in the standard

lowest order approximation

$$\chi(\vec{r}, E) \simeq [2\pi \bar{f}_E(0)/k] \int_{-\infty}^{\infty} dz\, \rho_0(\vec{x}), \qquad (3.2)$$

where $\bar{f}_E(0)$ is the forward pion-nucleon scattering amplitude averaged over the number of neutrons and protons in the target, and $\rho_0(\vec{x})$ is the ground state density normalized to unity. In addition, if we adopt the approximations discussed after Eq. (2.37), we need only consider the imaginary part of Eq. (3.2) as a function of radius. We write the imaginary part as

$$\chi^I(r, E) \simeq \bar{\sigma}(E)\Theta(r), \qquad (3.3)$$

where $\bar{\sigma}(E)$ is the averaged pion-nucleon total cross section and $\Theta(r)$ is the standard eikonal thickness function,

$$\Theta(b) = \tfrac{1}{2} \int_{-\infty}^{\infty} dz\, \rho_0(b^2 + z^2), \qquad (3.4)$$

treated as a function of radius.

The expression given by Eq. (3.3) will be used for χ in the following examples, with the laboratory pion-nucleon total cross sections[15] used to

calculate $\bar{\sigma}(E)$. This treatment of χ is admittedly naive; nevertheless, we will see that it provides us with the qualitatively correct energy-dependent attenuation.

C. Specific nuclear transitions

Given the fixed scatterer coefficients and a prescription for determining the attenuation factor, we are now ready to calculate pion-nucleus differential cross sections for specific nuclear transitions. Because there is a large amount of data for the $^{12}C(\pi, \pi')\,^{12}C^*$ reaction, we will display calculations for this reaction and compare our calculations to the data when appropriate.[16]

For the first example, we consider a stretched unnatural parity excitation of a $J_i = T_i = 0$ nucleus, which we will describe by a pure particle-hole configuration. Although such a description is certainly an oversimplification (for example, three-particle three-hole admixtures are ignored), it has been used successfully to reproduce the shapes of these states as seen by inelastic scattering of electrons and protons.[17] From Eqs. (2.1) and (2.26) we obtain for a stretched isoscalar transition

$$\frac{d\sigma^{J^-,0}}{d\Omega}(q, E, \theta) = \left[\frac{E(k')}{E(k)}\left(\frac{k'}{k}\right)^3\right] e^{q^2 b^2/2A}(2\pi)\sin^2(\theta)\,|\langle J00\,||\,\hat{S}^u_J(q,E)\,||\,000\rangle|^2. \qquad (3.5)$$

If we let α and β denote the particular particle and hole that couple to form this state of spin and parity J^-, we obtain from Eq. (2.38c)

$$|\langle J00\,||\,\hat{S}^u_J(q,E)\,||\,000\rangle|^2 = \left(\frac{3}{\pi}\right)|\bar{C}_1(E)|^2(J+1)(2J-1)(\bar{j}_\alpha\bar{l}_\alpha\bar{j}_\beta\bar{l}_\beta)^2$$

$$\times \begin{pmatrix} l_\alpha & J-1 & l_\beta \\ 0 & 0 & 0 \end{pmatrix}^2 \begin{Bmatrix} l_\alpha & \tfrac{1}{2} & j_\alpha \\ l_\beta & \tfrac{1}{2} & j_\beta \\ J-1 & 1 & J \end{Bmatrix}^2 (\bar{\alpha}\,|e^{-\chi}j_{J-1}|\,\bar{\beta})^2. \qquad (3.6)$$

Inserting Eq. (3.6) into (3.5), we may write the differential cross section for a stretched isoscalar state as

$$\frac{d\sigma^{J^-,0}}{d\Omega}(q, E, \theta) = \left[\frac{E(k')}{E(k)}\left(\frac{k'}{k}\right)^3\right]|\bar{C}_1(E)|^2\sin^2(\theta)\,\mathcal{F}^{str}_{J-1}(q, E), \qquad (3.7)$$

where for our particle-hole shell-model description

$$\mathcal{F}^{str}_L(q, E) \equiv e^{q^2 b^2/2A}(\bar{\alpha}\,|e^{-\chi}j_L|\,\bar{\beta})^2 N^{JL}_{str}, \qquad (3.8a)$$

and

$$N^{JL}_{str} = 6(J+1)(\bar{L}\bar{j}_\alpha\bar{j}_\beta\bar{l}_\alpha\bar{l}_\beta)^2 \begin{pmatrix} l_\alpha & L & l_\beta \\ 0 & 0 & 0 \end{pmatrix}^2 \begin{Bmatrix} l_\alpha & \tfrac{1}{2} & j_\alpha \\ l_\beta & \tfrac{1}{2} & j_\beta \\ L & 1 & J \end{Bmatrix}^2. \qquad (3.8b)$$

Now for a simple example of a low-spin state, we use the same particle and hole as above but couple them to form a natural parity isovector state. We then obtain from Eqs. (2.1), (2.6)–(2.28), and (2.38)

$$\frac{d\sigma^{J^\pi,1}}{d\Omega}(q, E, \theta) = \left[\frac{E(k')}{E(k)}\left(\frac{k'}{k}\right)\right]\left(\begin{Bmatrix} l_\alpha & j_\alpha & \tfrac{1}{2} \\ j_\beta & l_\beta & J \end{Bmatrix}^2\right)\left[|\bar{B}_0|^2 + \left(\frac{k'}{k}\right)2\,\mathrm{Re}\{\bar{B}_0\bar{B}_1^*\}\cos(\theta) + \left(\frac{k'}{k}\right)^2|\bar{B}_1|^2\cos^2(\theta)\right]$$

$$+\, 3(\bar{J})^2\begin{Bmatrix} l_\alpha & \tfrac{1}{2} & j_\alpha \\ l_\beta & \tfrac{1}{2} & j_\beta \\ J & 1 & J \end{Bmatrix}^2\left(\frac{k'}{k}\right)^2|\bar{D}_1|^2\sin^2(\theta)\Bigg)\,\mathfrak{F}_J^n(q, E)\,. \tag{3.9}$$

The natural parity form factor $\mathfrak{F}_J^n$, appearing in Eq. (3.9) is defined by Eq. (3.8a) with the normalization N_{str}^{JL} replaced by

$$N_{\text{nat}}^L = 2(\bar{L}\,\bar{j}_\alpha\bar{j}_\beta\bar{l}_\alpha\bar{l}_\beta)^2\begin{pmatrix} l_\alpha & L & l_\beta \\ 0 & 0 & 0 \end{pmatrix}^2. \tag{3.10}$$

Using the specific configuration $\bar{\alpha} = 1d_{5/2}$ and $\bar{\beta} = 1p_{3/2}$ in Eqs. (3.7) and (3.9), we have calculated the $J^\pi = 4^-$, $T = 0$ stretched state and a hypothetical $J^\pi = 1^-$, $T = 1$ state in ^{12}C. The oscillator parameter $b = 1.64$ fm was used in our calculations to determine the single-particle radial wave functions. In Fig. 3, we show the calculated differential cross sections for pion laboratory kinetic energies of 116, 180, and 260 MeV. The short-dashed curves are the numerical results of Eqs. (3.7) and (3.9), where we have used $\bar{\sigma}(180) = 136$ mb and $\bar{\sigma}(116) \simeq \bar{\sigma}(260) \simeq 61$ mb to calculate the form factors $\mathfrak{F}(q, E)$. We refer to these results as the "eikonal zero-range approximation" (EZRA). The long-dashed curves result from setting the distorted wave attenuation factor $\chi = 0$ in Eqs. (3.7) and (3.9). We label these results as the "plane wave zero-range approximation" (PWZRA). The solid curves in Fig. 3 have been obtained from a momentum space finite-range DWIA computer code.[9] This code uses the complete fixed scatterer pion-nucleon t matrix given in Eq. (2.3) and distorted waves obtained by solving the Klein-Gordon equation with the corresponding fixed scatterer optical potential.

By comparing the three different calculations shown in Fig. 3 we see that, although we have treated χ very simply, the EZRA does well in reproducing the magnitudes, shapes, and (except at 116 MeV) positions of the first maxima given by the DWIA. We also display some data in Fig. 3. This data is of a state at 19.25 MeV that has recently been observed in the ^{12}C(π^+, $\pi^{+\prime}$) ^{12}C* reaction. There is some reason to believe[18] that this state has a $J^\pi = 4^-$. The shapes of our calculated angular distributions certainly support the $J^\pi = 4^-$ assignment. However, the predictions of the fixed q, variable energy, and angle expressions obtained in Sec. II B offer us another check on the spin and parity of this state. We shall

give some examples of these fixed q plots next.

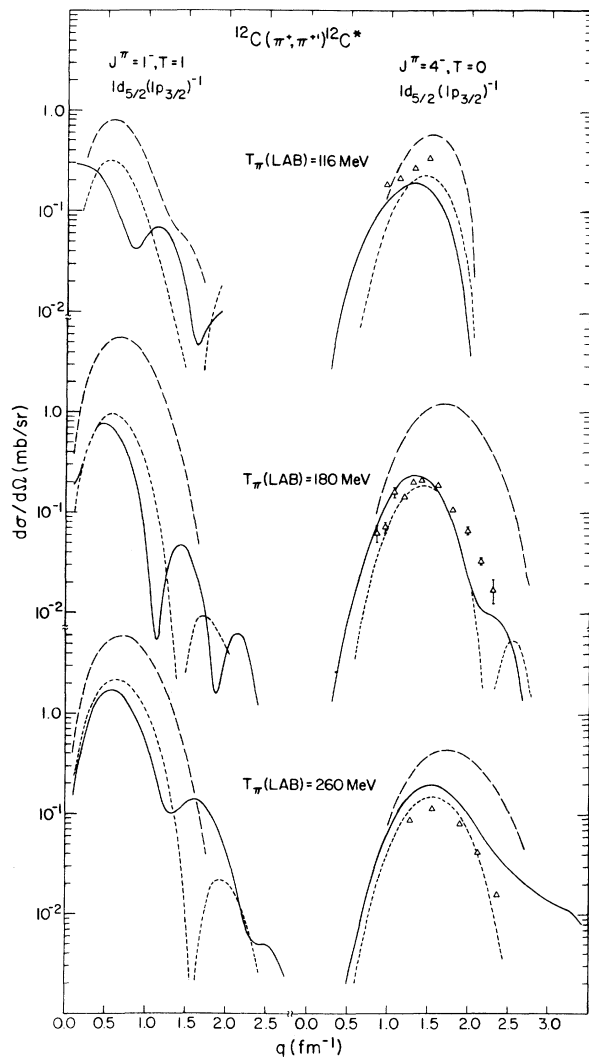From the discussion in Sec. II B, we found that the differential cross section for any unnatural

FIG. 3. Differential cross sections as a function of momentum transfer (q) for pion laboratory kinetic energies of 116, 180, and 260 MeV. The solid curves are the finite-range DWIA calculations, the long-dashed curves are the PWZRA calculations, and the short-dashed curves are the EZRA calculations discussed in the text. The data is from Ref. 16.

parity isoscalar transition could be written in a form similar to Eq. (3.7),

$$\frac{d\sigma^u}{d\Omega}(q, E, \theta) = \left[\frac{E(k')}{E(k)}\left(\frac{k'}{k}\right)^3\right]|\overline{C}_1(E)|^2\sin^2(\theta)\mathfrak{F}^u(q, E).$$

$$(3.11)$$

If we further assume that the P-wave non-spin-flip contribution to a natural transition dominates over all the other terms, we may write an expression similar to Eq. (3.9) for any natural parity isoscalar transition

$$\frac{d\sigma^n}{d\Omega}(q, E, \theta) \simeq \left[\frac{E(k')}{E(k)}\left(\frac{k'}{k}\right)^3\right]|\overline{A}_1(E)|^2\cos^2(\theta)\,\mathfrak{F}^n(q, E).$$

$$(3.12)$$

[For isovector transitions, we would replace $\overline{C}_1$ and $\overline{A}_1$ in Eqs. (3.1) and (3.12) by $\overline{D}_1$ and $\overline{B}_1$.]
Note that in these equations the energy dependence resulting from the basic two-body inelastic transition operator and the energy dependence resulting from the distorted waves are explicitly separated.

We now consider Eqs. (3.11) and (3.12) as functions of E at fixed $q = q_0$. To understand the energy dependence of these equations, we first consider the explicit energy dependences. For example, we define the plane wave energy-dependent factor for isoscalar unnatural parity transitions as

$$\Lambda_c(E) = \left[\frac{E(k')}{E(k)}\left(\frac{k'}{k}\right)^3\right]|\overline{C}_1(E)|^2.$$

$$(3.13)$$

The total explicit energy dependence of Eq. (3.11) is then the product of $\Lambda_c(E)$ and $\mathfrak{F}(q_0, E)$, which we denote [in accordance with Eq. (2.43)] as

$$\Gamma(E)\,\mathfrak{S}^2(q_0) = \Lambda_c(E)\,\mathfrak{F}(q_0, E).$$

$$(3.14)$$

In Fig. 4 we plotted the factors $\Lambda_c(E)$, $\mathfrak{F}(q_0, E)$, and their product for the stretched $J^\pi = 4^-$ state of ^{12}C considered above. For the factor $\mathfrak{F}(q_0, E)$, the value $q_0 \simeq 1.4\ \mathrm{fm}^{-1}$ was chosen because at $T_\pi \simeq 180\ \mathrm{MeV}$, $\mathfrak{F}(q, E)$ reaches a maximum at this value of q. [We use $T_\pi \simeq 180\ \mathrm{MeV}$ to determine q_0 because $\chi^R \simeq 0$ in this region, cf. Eq. (2.37).]
One vividly apparent feature in Fig. 4 is that the strong energy dependence of $\Lambda_c(E)$ is essentially negated by the behavior of $\mathfrak{F}(q_0, E)$. This behavior of the form factor at fixed q reflects the fact that the distorted wave attenuation factor modulates the amount of nuclear "volume" over which the nuclear transition density is integrated. In Fig. 5 we have illustrated this point by plotting the distorted nuclear transition density

$$d_{\alpha\beta}(r, E) = r^2 R_\alpha(r)R_\beta(r)e^{-\chi^I(r, E)},$$

$$(3.15)$$

for the stretched $J^\pi = 4^-$ state under consideration. For comparison, we show in Fig. 5 the undistorted transition density ($\overline{\sigma} = 0.0$) and the distorted tran-
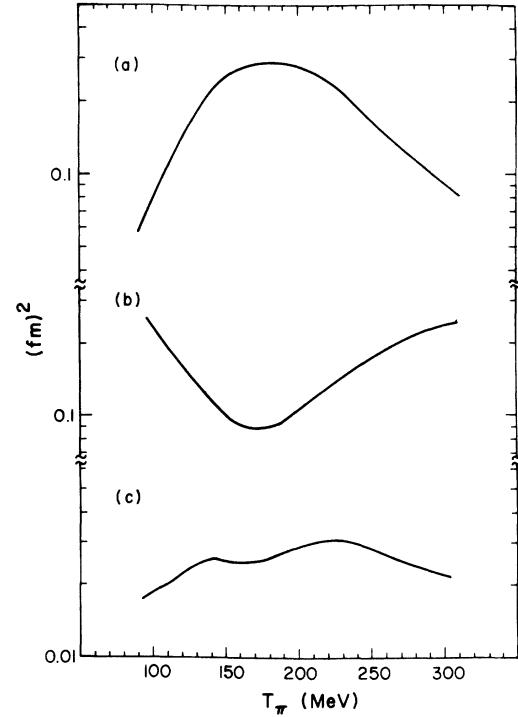

FIG. 4. The energy dependent factors: (a) $\Lambda_c(E)$ defined in Eq. (3.13) and representing the spin-flip isoscalar pion-nucleon coupling; (b) $F(q_0, E)$ defined in Eq. (3.8) and representing the nuclear form factor at a fixed momentum transfer of 1.4 fm^{-1} with $\overline{\alpha}$ $= 1d_{5/2}$, $\overline{\beta} = 1p_{3/2}$, $L = 3$, $J = 4$; and (c) the product of (a) and (b).
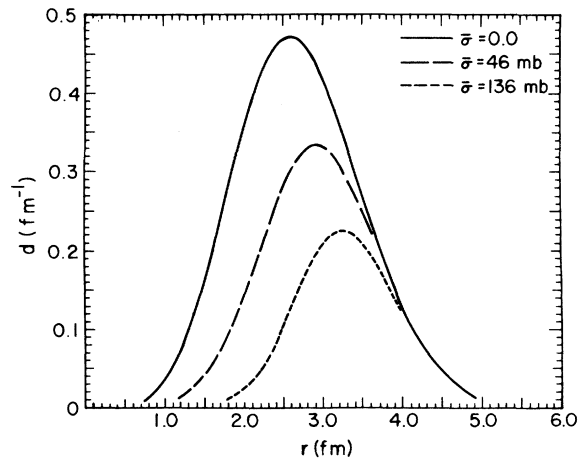

FIG. 5. The distorted nuclear transition density defined in Eq. (3.15) for $\alpha = 1d_{5/2}$, $\beta = 1p_{3/2}$. The solid curve is for the case of no distortion, the long-dashed curve is the case of distortion corresponding to pion kinetic energies of 100 or 300 MeV, and the short-dashed curve results from 180 MeV distortion.

sition densities correponding to pion kinetic energies of 100 and 300 MeV $[\bar{\sigma}(180) = 136$ mb$]$. The effects of distortions upon the transition density are to lower the magnitude and shift the peak position to larger values of radius as the kinetic energy approaches the resonance (either from above or below).

Now if we assume that the cancellation of the explicit energy dependences discussed above obtains for most inelastic transitions, then we arrive at some very simple predictions. That is, the essential energy dependence of differential cross sections at fixed q is the *implicit* energy dependences of Eqs. (3.11) and (3.12) yielding the relations

$$\frac{d\sigma^u}{d\Omega}(q_0, E, \theta) \propto \sin^2(\theta) \qquad (3.16)$$

and

$$\frac{d\sigma^n}{d\Omega}(q_0, E, \theta) \propto \cos^2(\theta), \qquad (3.17)$$

where

$$\cos(\theta) = \frac{(k')^2 + k^2 - q_0^2}{2k'k}. \qquad (3.18)$$

To show the behavior of the $\cos^2(\theta)$ and $\sin^2(\theta)$ terms at fixed q as a function of E, we have plotted them in Fig. 6(a) for different values of q. In Fig. 6(b) we have displayed fixed q $^{12}C(\pi, \pi')$ $^{12}C^*$ data for two well-known natural parity transitions [the $2^+(4.44$-MeV) state and the $3^-(9.64$-MeV) state] and for the 19.25-MeV state that we have previously treated as a 4^- unnatural parity transition. The values of q_0 for which we chose the data points were determined by the position of the first peak in the $T_\pi = 180$ MeV experimental angular distributions. We took $q_0 \simeq 0.75$, 1.0, and 1.41 fm^{-1} for the 2^+, 3^-, and 4^- states, respectively. If an energy of T_π other than 180 MeV had no datum point within 10% of the particular q_0 desired, we chose the closest datum point and labeled it with an arrow. The arrow indicates the direction in which that particular point should move if it were at the desired value of q. (This was determined by considering the behavior of the experimental angular distribution.) Although Eq. (3.17) is inherently less reliable than Eq. (3.16) (because we have dropped the spin-flip contribution to a natural parity transition), the qualitatively different behavior of the natural parity transitions from that of the proposed 4^- unnatural parity transition is consistent with our simple predictions.

Finally, we demonstrate the effects of the Fermi-motion correction terms, discussed in Sec. II C, by considering two examples of unnatural
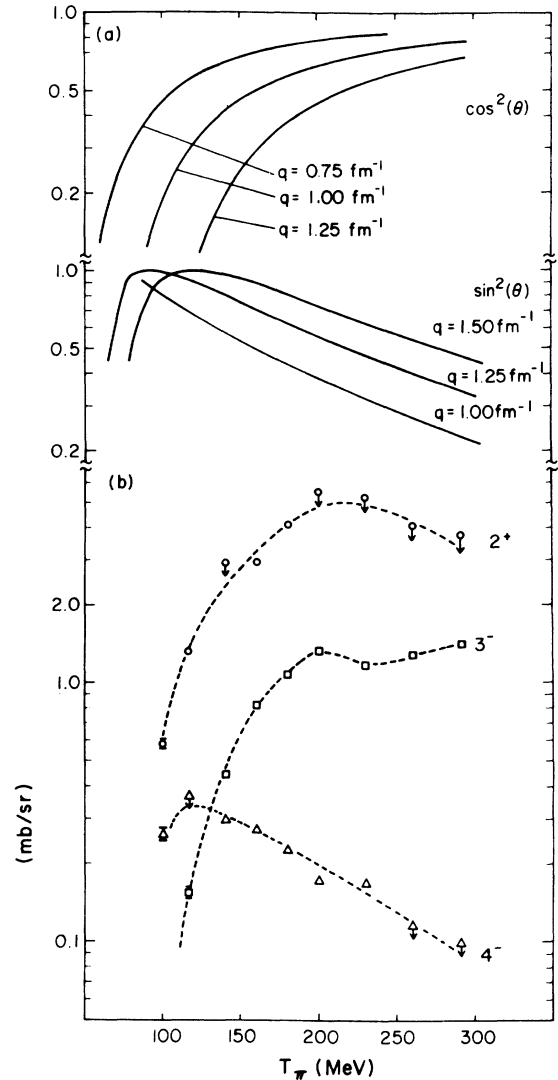

FIG. 6. Differential cross sections at fixed momentum transfer (q) as a function of pion laboratory kinetic energy. (a) Plots of $\cos^2(\theta)$ and $\sin^2(\theta)$ normalized to unity and calculated from Eq. (3.18) for the indicated values of q. (b) π^+ inelastic data for the $2^+(4.44$ MeV), $3^-(9.64$ MeV), and $4^-(19.25$ MeV) states of ^{12}C. The data is from Ref. 16. The dashed curves are to guide the eye.

parity states for which $\Delta J \leq L_{max}$. From Eqs. (2.1), (2.26), and (2.62) we may write the unpolarized inelastic differential cross section for an unnatural parity transition as

$$\frac{d\sigma^{fi}}{d\Omega}(q, \theta, E) = \left[\frac{E(k')}{E(k)}\left(\frac{k'}{k}\right)^3\right]\frac{e^{q^2b^2/2A}}{(2J_i + 1)}$$

$$\times [X(q, E)\sin^2(\theta) + Y(q, E)\cos^2(\theta)\cos^2(\theta/2)$$

$$- Z(q, E)\sin(2\theta)\cos(\theta/2)], \qquad (3.19)$$

where

$$X(q,e) \equiv (2\pi)\left(\frac{k}{k'}\right)^2 F_\sigma{}^2 , \qquad (3.20)$$

$$Y(q,E) \equiv (2\pi)\left(\frac{k}{k'}\right)^2 F_c{}^2 , \qquad (3.21)$$

and

$$Z(q,E) \equiv (2\pi)\left(\frac{k}{k'}\right)^2 \{\mathrm{Re}\, F_\sigma F_c^*\} . \qquad (3.22)$$

In general, the factors F_σ and F_c [defined by Eqs. (2.28) and (2.63)] are given in terms of a multipole expansion over reduced matrix elements. For a $J_i = T_i = 0$ nucleus, however, a single term in each multipole series contributes. In this case

$$X(q,E) = (2\pi)|\langle J\, T0\,||\hat{S}_J^u||\,000\rangle|^2 , \qquad (3.23)$$

$$Y(q,E) = (2\pi)\left(\frac{k'}{k}\right)(k)^2 |\langle J\, T0\,||\hat{\mathcal{I}}_J^u||\,000\rangle|^2 , \qquad (3.24)$$

and

$$Z(q,E) \equiv (2\pi)\left(\frac{k'}{k}\right)^{1/2}(k)\,\mathrm{Re}\,\{\langle J\, T0\,||\hat{S}_J^u||\,000\rangle \\ \times \langle J\, T0\,||\hat{\mathcal{I}}_J^u||\,000\rangle^*\} , \qquad (3.25)$$

for a final nuclear state of spin J and isospin T.

Now in the detailed expressions for the reduced matrix elements [Eqs. (2.38c) and (2.65a)], we intend to use simple harmonic oscillator radial wave functions. Because oscillator radial wave functions depend only upon the principal and orbital quantum numbers, we may eliminate the sums over the total angular momenta j_α and j_β by using the L-S coupled structure constants

$$\eta_{LS}^{JT}(\overline{\alpha},\overline{\beta}) \equiv \tilde{L}\tilde{S} \sum_{j_\alpha j_\beta} \hat{j}_\alpha \hat{j}_\beta \begin{Bmatrix} l_\alpha & l_\beta & L \\ \tfrac{1}{2} & \tfrac{1}{2} & S \\ j_\alpha & j_\beta & J \end{Bmatrix} \xi_{JT}^{fi}(\overline{\alpha},\overline{\beta}) . \qquad (3.26)$$

For example, the reduced matrix elements needed in Eqs. (3.23)–(3.25) for isoscalar transitions may be written as [cf. Eqs. (2.38c) and (2.65a)]

$$\langle J\,00||\,S_J^u(q,E)||\,000\rangle = \frac{i\overline{C}_1}{\sqrt{\pi}} \sum_{n_\alpha l_\alpha,\, l_\beta l_\beta} (-)^{l_\alpha} \tilde{l}_\alpha \tilde{l}_\beta \sum_L \begin{pmatrix} l_\alpha & L & l_\beta \\ 0 & 0 & 0 \end{pmatrix} \eta_{L1}^{J0}(n_\alpha l_\alpha, n_\beta l_\beta)$$

$$\times [\,(J+1)^{1/2}\delta_{L,\,J-1} - \sqrt{J}\,\delta_{L,\,J+1}\,](n_\alpha l_\alpha |\,e^{-x}j_L\,|n_\beta\, l_\beta) \qquad (3.27)$$

and

$$\langle J\,00||\,\hat{\mathcal{I}}_J^u(q,E)||\,000\rangle = (-)^J \frac{i}{m_N}\left(\frac{\partial}{\partial E}\,\overline{A}_1\right)\frac{(\tilde{J})^2}{\sqrt{\pi}} \sum_{n_\alpha l_\alpha,\, n_\beta l_\beta} \tilde{l}_\alpha(\tilde{l}_\beta)^{-1}\eta_{J0}^{J0}(n_\alpha l_\alpha, n_\beta l_\beta) R_{JJ}^{\alpha\beta}(q,t) . \qquad (3.28)$$

(For isovector transitions, we replace $\overline{A}$ and $\overline{C}$ in these equations by $\overline{B}$ and $\overline{D}$.)

Two examples of unnatural parity transitions that satisfy the criterion of $\Delta J < L_{\max}$ are the $J^\pi = 1^+$ and $J^\pi = 2^-$ isoscalar transitions in ^{12}C. We assume the structure of the 1^+ state results from transitions within the $1p$ shell, whereas the 2^- state may be described as a transition from the $1p$ shell to the $2s$-$1d$ shell. Adopting such descriptions, we obtain from Eqs. (3.27) and (3.28) the reduced matrix elements

$$\langle 100||\,\hat{S}_1^u||\,000\rangle = i\,\frac{\sqrt{6}}{\sqrt{\pi}}\,\overline{C}_1\left[\eta_{01}^{10}(11|e^{-x}j_0|11) + \frac{\eta_{21}^{10}}{\sqrt{5}}(11|\,e^{-x}j_2|11)\right] \qquad (3.29)$$

and

$$k\langle 100||\,\hat{\mathcal{I}}_1^u||\,000\rangle = i\,\frac{\sqrt{6}}{\sqrt{\pi}}\left(\frac{k}{bm_N}\,\frac{\partial A_1}{\partial E}\right)\eta_{10}^{10}\,(11|e^{-x}j_1|10) \qquad (3.30)$$

for the $J^\pi = 1^+$, $T = 0$ transition, and

$$\langle 200||\,\hat{S}_2^u||\,000\rangle = i\,\frac{\sqrt{6}}{\sqrt{\pi}}\,\overline{C}_1\left[\eta_{11}^{20}(2,1)(12|e^{-x}j_1|11) + \frac{\sqrt{3}}{\sqrt{7}}\,\eta_{31}^{20}(2,1)(12|e^{-x}j_3|11) - \frac{\eta_{11}^{20}(0,1)}{\sqrt{2}}(20|\,e^{-x}j_1|11)\right] \qquad (3.31)$$

and

$$k\langle 200||\,\hat{\mathcal{I}}_2^u||\,000\rangle = i\,\frac{\sqrt{10}}{\sqrt{\pi}}\left(\frac{k}{bm_N}\,\frac{\partial A_1}{\partial E}\right)\eta_{20}^{20}(2,1)(12|\,e^{-x}j_2|10) \qquad (3.32)$$

for the $J^\pi = 2^-$, $T = 0$ transition. We note that be-
cause the nuclear current does not involve the
Pauli spin operator [and consequently $S = 0$ in Eq.
(3.28)], only the $1d$-$1p$ components of the $J^\pi = 2^-$
state contribute to Eq. (3.32). Later we will dem-
onstrate how this particular feature may prove
useful.

Before we can calculate cross sections for these
particular transitions [by inserting the above ex-
pressions for the reduced matrix elements into
Eqs. (3.23) through (3.25)], we need to adopt some
nuclear structure model so as to obtain numerical
values for the η's. Different nuclear structure
models will ultimately yield different cross sec-
tions. One quantity that does not depend upon the
specific nuclear structure, however, is the pion-
nucleon Fermi-motion coupling term

$$g(E) \equiv \frac{k}{bm_N} \left(\frac{\partial \overline{A}_1}{\partial E} \right). \tag{3.33}$$

To illustrate the energy-dependence of the Fermi-
motion coupling as compared to that of the spin-
flip coupling, we have plotted in Fig. 7 the terms
$|\overline{C}_1|^2$, $|g|^2$, and $\text{Re}\{\overline{C}_1 g^*\}$, which result from
the X, Y, and Z terms in Eq. (3.19). We find,
in agreement with Wilkin, that the magnitudes of
the Fermi-motion couplings are comparable to the
spin-flip coupling and the "interference" term
$\text{Re}\{\overline{C}_1 g^*\}$ changes sign as we go from below to
above the $(3,3)$ resonance. The extent to which
the Fermi-motion coupling affects the pion-nu-
cleus cross section will depend upon the relative
strength of the multiplicative nuclear factors.

For the $J^\pi = 1^+$ state, we begin by assuming
that the η's are determined by a pure j-j coupled
$1p_{1/2}(1p_{3/2})^{-1}$ particle-hole configuration. With

this simple structure we obtain from Eq. (3.26)
$\eta^{10}_{01} = (\frac{2}{3})^{3/2}$, $\eta^{10}_{21} = (\frac{5}{54})^{1/2}$, and $\eta^{10}_{10} = -\frac{1}{3}$. Using these
structure constants in Eqs. (3.29) and (3.30), we
have calculated differential cross sections by
using Eq. (3.19). In Fig. 8 we display our results
as a function of q for pion kinetic energies of 120,
180, and 240 MeV. In Fig. 9(a) we plot our re-
sults as a function of kinetic energy at a fixed
momentum transfer of 0.5 fm^{-1}. The solid curves
in both figures are calculations without the Fer-
mi-motion terms [$Y = Z = 0$ in Eq. (3.19)], and the
long-dashed curves include the Fermi-motion
terms. The short-dashed curve in Fig. 9(a) is the
$\sin^2(\theta)$ approximation normalized to the 100-MeV
differential cross section without Fermi-motion
terms. In these figures we have also included
some recent data taken on the $J^\pi = 1^+$, $T = 0$ state
of ^{12}C located at 12.71 MeV.
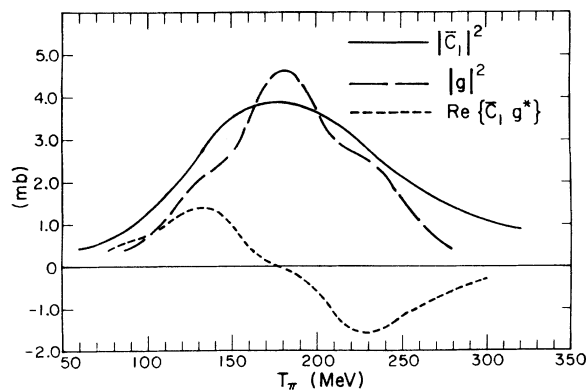
We see that for this particular state one of the

FIG. 7. Comparison of the pion-nucleon couplings
that result from the Fermi-motion terms. The solid
curve is the square of the spin-flip isoscalar coupling,
the long-dashed curve is the square of the Fermi-motion
coupling defined by Eq. (3.33), and the short-dashed
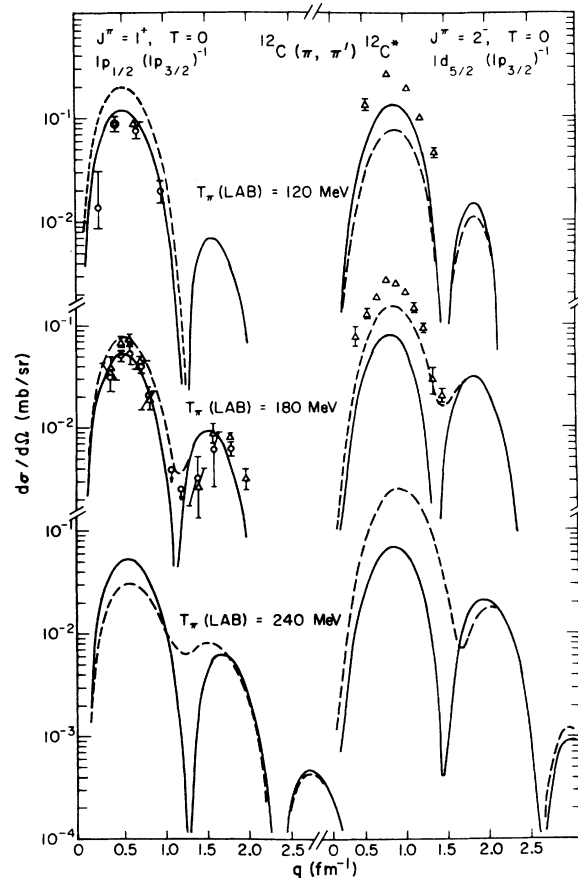curve is the interference term.

FIG. 8. Differential cross sections as a function of
momentum transfer (q) for pion laboratory kinetic
energies of 120, 180, and 240 MeV. The solid curves
are the EZRA calculations without the Fermi-motion
terms and the dashed curves are the EZRA calculations
including the Fermi-motion terms. The data is from
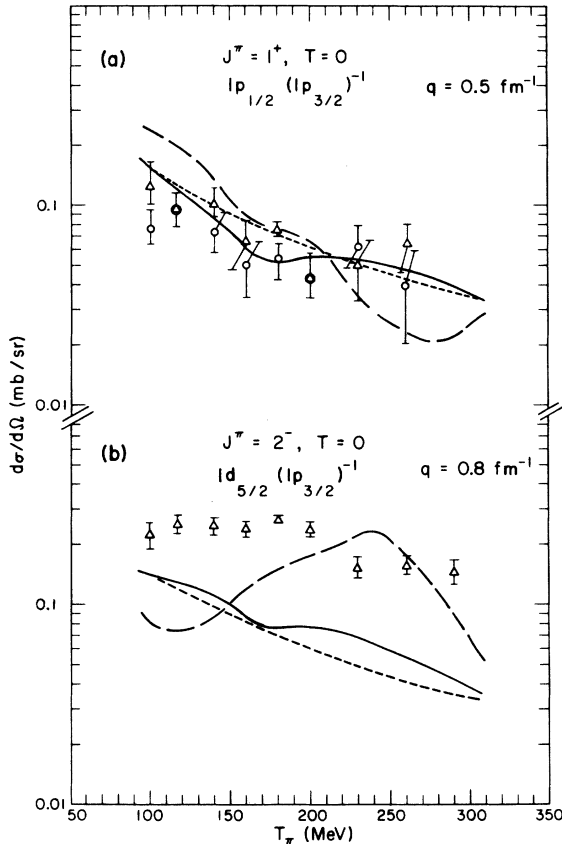Cottingame ($\triangle$) and Peterson ($\circ$) of Ref. 16.

FIG. 9. Differential cross sections at fixed momentum transfer (q) as a function of pion laboratory kinetic energy. The solid curves are the EZRA calculations without the Fermi-motion terms, the long-dashed curves are the EZRA calculations including the Fermi-motion terms, and the short dashed curves are the $\sin^2(\theta)$ approximation normalized to the solid curves at 100 MeV. The data is from Cottingame ($\triangle$) and Peterson (o) of Ref. 16. The transitions are the (a) $J^{\pi}=1^{+}$, $T=0$, 12.71 MeV state and (b) $J^{\pi}=2^{-}$, $T=0$, 18.36 MeV state in ^{12}C.

effects of including Fermi-motion terms is to increase the first maximum of the differential cross section below $T_{\pi} \simeq 210$ MeV and decrease it above 210 MeV. The changes involved can be as much as a factor of 1.7 increase around $T_{\pi} \simeq 120$ MeV and a factor of 2.1 decrease around $T_{\pi} = 260$ MeV. By comparing our calculations to the data in Fig. 8, we see that (with or without the Fermi-motion terms) the shapes and positions of the first peaks are in excellent agreement. Given the uncertainties in the data used for the fixed q plots in Fig. 9(a), all we can deduce is that the general trend of the data is consistent with our calculations. We wish to point out, however, that the absolute magnitudes of our calculations should not be taken too seriously. Besides an uncertainty due to our simple treatment of the distorted wave attenua-

tion factor, there is a nuclear structure renormalization that must be included. Just as in the case of inelastic electron scattering[7] over the region of the first peak the pure particle-hole results should be reduced without appreciably altering the q dependence.

To demonstrate that a more realistic treatment of the nuclear structure tends only to change the magnitude of our results, we have also calculated this transition by using the wave functions of Cohen and Kurath.[19] The structure coefficients for this case can be obtained directly from the tables of Ref. 4, and they are (omitting an overall phase) $\eta_{01}^{10} = 0.215$, $\eta_{21}^{10} = 0.069$, and $\eta_{10}^{10} = 0.132$. The results obtained with these "more sophisticated" structure coefficients are qualitatively the same as those depicted in Figs. 8 and 9, except for an overall normalization. This is due to the relative insignificance of the $L = 2$ as compared to the $L = 0$ contribution to the spin-flip term for $q \lesssim 1$ fm^{-1}. [See Eq. (3.29).] Ignoring the $L = 2$ structure coefficient, we note that both the $L = 0$ and $L = 1$ Cohen-Kurath coefficients are a factor of 2.53 smaller than the corresponding particle-hole coefficients. Thus, the relative weighting of the Fermi-motion term [Eq. (3.30)] as compared to the spin-flip term [Eq. (3.29)] is the same for either nuclear structure model. The only difference between nuclear models is an overall normalization.

For the $J^{\pi} = 2^{-}$ state, we have calculated differential cross sections assuming that the η's appearing in Eqs. (3.31) and (3.32) result from a pure $j-j$ coupled $1d_{5/3}(1p_{3/2})^{-1}$ particle-hole configuration. These results are shown in Figs. 8 and 9(b). In Fig. 8 we have plotted the cross sections as a function q at fixed values of kinetic energy, whereas in Fig. 9(b) we display our results as a function of kinetic energy at a fixed value of $q = 0.8$ fm^{-1}. We also display some data along with our calculations. This data is of a state at 18.36 MeV that has recently been observed and speculated to have a $J^{\pi} = 2^{-}$, $T = 0$.[20] The shapes of our angular distributions calculated with a pure $1d_{5/2}(1p_{3/2})^{-1}$ particle-hole are consistent with the data. We have also calculated differential cross sections for this transition by assuming a pure $2s_{1/2}(1p_{3/2})^{-1}$ particle-hole configuration. The resulting shapes of the first peaks are essentially the same as those obtained with the $1d_{5/2}(1p_{3/2})^{-1}$ configuration. Therefore, from a single angular distribution, one cannot determine which configuration dominates this state. However, by looking at the fixed q plots in Fig. 9(b) we can distinguish between them. That is, if this transition has a dominant $1d_{5/2}(1p_{3/2})^{-1}$ component, the differential cross section at fixed q would be drastically different

from the simple $\sin^2(\theta)$ dependence. If this transition has a dominant $2s_{1/2}(1p_{3/2})^{-1}$ component, then there would be no Fermi-motion terms and the differential cross section at fixed q would essentially follow the $\sin^2(\theta)$ rule. Because the data do not differ extremely from the $\sin^2(\theta)$ dependence, our results suggest that this transition has a dominant $2s_{1/2}(1p_{3/2})^{-1}$ particle-hole component.

IV. SUMMARY AND DISCUSSION

In this section we review the motivation for the investigation leading to the results contained in this paper, summarize the results, and suggest further experimental and theoretical research that would test or extend the ideas presented herein. The qualitative agreement between the initial (π, π') experiments and the DWIA theoretical predictions suggests that such a theory may contain much of the important physics. This is somewhat surprising and indicates that more stringent tests of the approach be investigated. We note, however, that refinement of the simple theory by including more realistic distortions and the effects of local field corrections or isobar-medium interactions, may still be cast within a DWIA framework. Thus, it seems useful to separate the various contributions of the DWIA—distortion, transition operator, and nuclear structure—and study their dependences on pion energy (E), laboratory scattering angle (θ), and three-momentum transfer (q). These variables are especially useful because the nuclear form factors are functions only of q (as in electron and proton inelastic scattering studies), whereas the reaction mechanism has strong E and θ dependences even at fixed q. The explicit angle dependence of the transition operator arises from the multiplication of q and energy dependent scalars by various scalar products of spin, relative coordinate, and momentum vectors. One goal of our studies on the q, E, and θ dependences discussed in this paper is to suggest ways to present experimental data so that different aspects of the theory are accentuated.

To obtain a simple separation of the various components of the theory, we assumed eikonal distored waves and zero-range S-wave and P-wave fixed scatterer pion-nucleon input for the transition operator. We then expressed the matter-density and spin-density operators of Eqs. (2.14) and (2.15) in terms of irreducible tensor operators. This enabled us to separate the transition operators for the nuclear space into those responsible for natural parity $[\hat{M}_{J\lambda}(q,E)$, $\hat{S}_{J\lambda}^{n}(q,E)]$ and unnatural parity $[\hat{S}_{J\lambda}^{u}(q,E)]$ transitions. Our basic result for unpolarized pion-nucleus inelas-

tic scattering given in Eqs. (2.26)–(2.29) thus followed. These expressions explicitly separate the partial-wave multipole spin- and matter-density contributions to inelastic scattering and reveal the characteristic q, E, and θ dependences associated with various pieces comprising the differential cross section.

In Sec. II B we discussed how the variation of E at fixed q (a set of experiments feasible at modern pion factories) could be used to isolate different contributions to the cross section. For example, in Eq. (2.45) an expression was given which allows one to obtain the P-wave spin-flip contribution as the slope of a straight line and the P-wave non-spin-flip piece as the extrapolated x intercept. Deviations from the straight line would give evidence that the underlying formalism is inadequate. Analogous expressions containing the S-wave piece were also discussed for natural parity states. Once a natural parity transition has been identified, one could use Eq. (2.47) to separate (with a slight model dependence) the S-wave and P-wave spin- and non-spin-flip contributions by working first at $\theta = 90°$ and then at small angles. These equations were used in Sec. III to compare with recent data on $^{12}C(\pi, \pi')^{12}C^*$. The results indicate that the techniques suggested should be useful in isolating various channel reaction contributions to inelastic scattering or, if unknown, aid in the determination of the parity of final nuclear states.

We also have noted in Sec. II B that the characteristic angle dependence associated with natural parity and unnatural parity transitions causes a difference (as a function of energy) in angle-integrated differential cross sections at fixed projectile energy loss. The dominance of angle-integrated natural parity transitions over unnatural parity transitions as the projectile energy increases results from two features: the $\cos^2(\theta)$ $[\sin^2(\theta)]$ dependence associated with P-wave dominated natural (unnatural) parity transitions, and the increasingly forward peaking of the q-dependent nuclear form factor.

The dependence of the pion-nucleon interaction on the total energy and relative momentum in the two-body center of mass frame results in an effective pion-nucleon current-current interaction (like the electron-nucleon convection current). Calculations to date of pion-nucleus inelastic scattering ignore the motion of the struck nucleon in the nucleus for the P-wave spin-flip pion-nucleon interaction. To treat this term correctly would require *not* making the "$t\rho$ factorization" approximation and actually performing the associated six-dimensional integral (as was done, for example, in our earlier model calculations of elastic scattering[12]). Such a procedure seems

prohibitively lengthy with present computers; therefore, in Sec. IIC we generalized an argument previously used by Wilkin[13] for approximately treating the Fermi motion of the target nucleons. This treatment involves a Taylor series expansion of the pion-nucleon transition operator about the point where the struck nucleon is at rest. The first term obtained is the usual approximation, whereas the second term involves the projectile energy derivative of the pion-nucleon t matrix and represents a Fermi-motion correction term. We have studied this correction term for unnatural parity transitions arising from the non-spin-flip part of the transition operator and it results in a convection current-type coupling mentioned above.

As a function of pion energy, the Fermi-motion term can interfere constructively or destructively with the usual spin-flip term depending on the sign of $\partial t_{\pi N}/\partial E$. This gives rise to a nonvanishing contribution to unnatural parity transitions at forward angles. Furthermore, the Fermi-motion term cannot affect stretched states and has a relative q dependence between it and the usual spin-flip term that differs from the relative q dependence between the magnetization and convection current densities in electron scattering. The numerical results of Sec. III suggest that the effect of Fermi motion could be measured by the appropriate energy variation studies and may be useful to further elucidate nuclear structure.

To utilize the fixed q suggestions we have presented here, initial experimental efforts should probably concentrate on light nuclei with $A \lesssim 40$. We make this recommendation for the following reasons: The density of final states is relatively less dense than in heavier targets, there is ample collaborative electromagnetic interaction data, and distortions are *relatively* less important. Targets with $J_i \neq 0$ should be included in such studies. The values of q selected should be near the maximum of the differential cross section and, in any event, should not be too low ($q \gtrsim 0.75$ fm^{-1}) because of the uncertainty in our present treatment of distortions at low momentum transfer.

The first investigation should establish whether or not the techniques suggested here can be used with a high degree of confidence to determine the parity of the final nuclear state for a variety of spins and targets. This means that initially, the parity of the state studied should be known from other reactions. Of course, it would be an added bonus if new states, whose spin and parity are uncertain, were identified in the same studies. This is not necessarily impossible because of the ability of pions to strongly excite spin-flip, $\Delta T = 0$ states at all momentum transfers. The next

set of experiments could be used to test the straight line Rosenbluth plot ideas we presented. In fact, if one has knowledge of the appropriate nuclear form factors, e.g., from electron scattering, then information regarding the effective S-wave and P-wave transition operators can be obtained. Finally, at some future time, experiments could be undertaken to study the Fermi motion induced convection current contributions discussed. For now, these corrections represent additional theoretical considerations that should be included in the theory before detailed comparison is made with experimental data.

Because the Fermi-motion corrections discussed in this paper depend crucially upon the energy dependence of the two-body input (i.e., the width of the resonance and whether it is an s-channel or t-channel resonance), it would be interesting to apply the idea to other reactions. In particular, kaon induced inelastic scattering and strangeness exchange reactions seem attractive areas for study because of the associated resonances involved. In fact, we have already begun such a study including consideration of excitation of unnatural parity states at forward angles because of such corrections.

Future theoretical work could include studying the effect of more realistic effective transition operators on the predictions. In particular, more detailed and realistic studies of the approximate distorted waves at low momentum transfer and effective transition operators including local field corrections and/or isobar-medium corrections will result in better theoretically motivated input into the expressions presented here. The important point is that, except for possible additional angle-transformation coefficients required if fixed scatterer input is not adopted, more realistic input can easily be accommodated in the framework we have discussed above. Once included, assuming the nuclear structure is known as discussed above, experiments using the energy variability of the current accelerators can more critically test the distorted wave effective t-matrix approximation. Once this is accomplished, the pion, using its unique interaction with the nucleus, could be an especially important additional probe of nuclear structure.

*Present address: Nuclear Physics Laboratory, University of Colorado, Boulder, Colo. 80309.

[1]H. K. Lee and H. McManus, Nucl. Phys. A167, 257 (1971).

[2]T.-S. H. Lee and F. Tabakin, Nucl. Phys. A226, 253 (1974).

[3]A. T. Hess and J. M. Eisenberg, Nucl. Phys. A241, 493 (1975).

[4]C. Olmer et al., Phys. Rev. Lett. 43, 612 (1979).

[5]T.-S. H. Lee and D. Kurath, Phys. Rev. C 21, 293 (1980); 22, 1670 (1980).

[6]T.-S. H. Lee and R. D. Lawson, Phys. Rev. C 21, 679 (1980).

[7]T. deForest, Jr. and J. D. Walecka, Adv. Phys. 15, 1 (1966).

[8]M. G. Piepho and G. E. Walker, Phys. Rev. C 9, 1352 (1974).

[9]M. K. Gupta and G. E. Walker, Nucl. Phys. A256, 444 (1976).

[10]Ian E. McCarthy and Kerek L. Pursey, Phys. Rev. 122, 578 (1961).

[11]For another technique see, for example, R. H. Landau, S. C. Phatak, and F. Tabakin, Ann. Phys. (N. Y). 78, 299 (1973).

[12]E. R. Siciliano and G. E. Walker, Phys. Rev. C 13, 257 (1976).

[13]C. Wilkin, Nucl. Phys. A220, 621 (1974).

[14]J.-F. Germond and Mikkel B. Johnson, Phys. Rev. C 22, 1622 (1980).

[15]V. S. Zidell, R. A. Arndt, and L. D. Roper, Virginia Polytechnic Institute report (unpublished).

[16]W. Cottingame et al. (private communication); C. L. Morris, Proceedings of the Workshop on Nuclear Structure with Intermediate-Energy Probes, 1980, Los Alamos Scientific Laboratory Report No. LA-8303-C; R. J. Peterson et al., Phys. Rev. C 21, 1030 (1980). Error bars are indicated only when they extend beyond the symbol used for the data.

[17]R. A. Lindgren et al., Phys. Rev. Lett. 42, 1524 (1979).

[18]E. R. Siciliano, Proceedings of the LAMPF Workshop on Pion Single Charge Exchange, 1979, Los Alamos Scientific Laboratory Report No. LA-7892-C.

[19]S. Cohen and D. Kurath, Nucl. Phys. 73, 1 (1965).

[20]C. L. Morris, Proceedings of the Workshop on Nuclear Structure with Intermediate-Energy Probes, 1980, Los Alamos Scientific Laboratory Report No. LA-8303-C.